1974

Ionospheric Gravity Wave Effects On The Angle Of Arrival Of Solar Metric Radio Waves

Charles Warren Colpitts

IONOSPHERIC GRAVITY WAVE EFFECTS ON THE ANGLE OF ARRIVAL OF SOLAR METRIC RADIO WAVES

by

Charles Warren Colpitts

Department of Physics

Submitted in partial fulfillment

of the requirements for the degree of

Doctor of Philosophy

Faculty of Graduate Studies

The University of Western Ontario

London, Canada

May, 1974

ABSTRACT

Angle of arrival measurements of solar radio waves frequently exhibit large-scale fluctuations, sometimes attributed to motions in the sun's atmosphere. Solar interferometer observations were made at 50 and 150 MHz as well as satellite beacon angle of arrival measurements at the higher frequency. It is shown that a great many large-scale variations are caused by gravity wave induced travelling disturbances in the terrestrial ionosphere.

Techniques of spectral analysis and a three-dimensional treatment of the focussing of radio waves by large ionospheric irregularities are used in the interpretation of the results. The use of the sun as a radio beacon to study the ionosphere is also discussed.

ACKNOWLEDGEMENTS

The author wishes to thank his supervisor, Dr. J.A. Fulford, for his continued support throughout the course of this work and for his guidance and criticism during the preparation of this thesis. The author also wishes to thank Dr. J. Jones and Dr. H.R. Froelich for their interest and advice, Dr. R.P. Lowe for providing a copy of the fast Fourier transform computer program and for assistance in its use, and a colleague, (now Dr.) M.J. Curry for many interesting discussions concerning the spectral analysis.

Financial assistance through a Province of Ontario Graduate Fellowship is gratefully acknowledged. The work was supported by a grant from the National Research Council.

TABLE OF CONTENTS

LIST OF TABLES

LIST OF FIGURES

CHAPTER 1

INTRODUCTION

Radio waves from the sun were first detected in the early 1940's, and since then many techniques have been developed for their observation over a wide range of frequencies (see, for example, Kundu, 1965). The development of the interferometer enabled experimenters to determine the positions of radio sources and in many cases to correlate them with optical features on the sun's surface. However, in the case of metric radio waves, variations were sometimes found to occur in the relative angle of arrival measurements (Wild et al, 1959, Warwick, 1968), casting doubt on the accuracy of the knowledge of the position of the source. Wild et al attributed periodic fluctuations to ionospheric refraction and averaged them out, while Warwick suggested that the variation was too large to be caused by the ionosphere. Source positions can be well established using very high frequencies, but the phenomena observed can be different at different wavelength regions. Knowledge of parameters observed at 50 MHz must be found at that frequency, not at several GHz.

Single frequency measurements made at this institution led to the suggestion that many motions apparently in the sun's atmosphere could be attributed to terrestrial ionospheric sources. This thesis describes an experiment to find evidence in support of this suggestion and it does show that a particular type of ionospheric motion, namely the

gravity-wave induced travelling ionospheric disturbance, causes large fluctuations in the angle of arrival of solar metric radio waves.

In view of the relevance of travelling ionospheric disturbances to this study, it is useful to indicate methods of their observation and values of the parameters which describe them.

1.1 Observations of Travelling Disturbances

The periodic nature of the fluctuations of a number of parameters indicate the presence of wave motion in the ionosphere, as was pointed out by Pierce and Mimno (1940) when they were studying F-layer reflections. Since then, many workers have observed large scale disturbances which appear to travel over large distances in the ionosphere.

These travelling ionospheric disturbances, or TID's as they have come to be known, have been studied by a number of investigators and a variety of methods. These include the backscatter radar (Tveten, 1961, Wickersham, 1965), vertical incidence ionosonde (Heisler, 1963), Thomson scatter, or, more correctly, incoherent scatter (Thome, 1964 and 1968), Vasseur and Waldteufel, 1969), Doppler sounder (Davies and Baker, 1966, Georges, 1968, Herron, 1973), the monitoring of electron content, usually measured by Faraday rotation (Titheridge, 1968, Rao and Yeh, 1968, Davis and DaRosa, 1969); and angle of arrival (Litva, 1972, MacDougall, 1972). A sample of some representative speeds, periods, and wavelengths is found in Table 1.1. Also it has been reported that time variations, characteristic of TID periods, have been observed in the apparent position of radio stars (Lawrence and Jespersen, 1961) and of the sun (Wild, et al, 1959).

Travelling ionospheric disturbances can be classified into three

TABLE 1-1

Experimenters	Speed (m/sec)	Periods (minutes)	Wavelength (km)
Beynon (1948)	120		
Munro (1950, 1953, 1958)	50 - 250	10 - 60	50 - 500
Bramley and Ross (1951)	80 - 170	to 30	several hundred
Hewish (1952)	100 - 300		
Bramley (1953)	40 - 360; mean 170		50 - 400; mean 180
Price (1954)	30 - 320; most at 170		
Toman (1955)	70 - 170		
Munro and Heisler (1956)	70 - 200		
Heisler	100 - 200		
Tveten (1961)	40 - 200; median 140		160 - 200 most frequent
Chan and Villard (1962)	400 - 750	30 - 90	1300 - 2000
Bowman (1968)		5 - 60	25 - 350
Titheridge (1968)		15 - 60	40 - 160
Reddi and Rao (1971)	40 - 230	3 - 39	

major groups (see, for example, the review article by Vasseur, et al, 1972). Large scale disturbances have periods of 30 minutes to about three hours, wavelengths of a few thousand kilometers, and travel mainly equatorward with high speeds, typically 400 to 800 m/sec. Medium scale disturbances have periods of 10 to 30 minutes, horizontal scale sizes of 100 to 200 kilometers, speeds of 100 to 200 m/sec, and no preferred direction of travel although a seasonal variation has been suggested. Many of the observations listed in Table 1.1 fall into this category. The third class are the short period oscillations and are characterized by very short (3-5 minutes) periods. This type is indicated in Table 1.1, and is also the type observed by Rao, et al, (1969).

1.2 Gravity Waves

The atmosphere, as a fluid, may contain different types of wave motion. Waves may exist on and propagate along a surface of discontinuity, as on a water surface bounded by air. These waves are called surface waves and are characterized by an imaginary wave number in the direction normal to the surface, signifying an exponential decrease in amplitude with distance away from the surface. The fluid body itself may contain waves whose horizontal and vertical wave numbers both have real components, so that the waves are able to propagate throughout the fluid. These are termed internal waves.

Acoustic waves in the atmosphere are internal waves driven by the force of compression and inertia and are longitudinal in nature. When the force of gravity becomes significant in affecting the propagation of the wave, the waves are no longer essentially longitudinal, but

have vertically transverse components, and the term acoustic-gravity wave, or simply gravity wave, is applied. There is now general agreement that TID's are ionospheric manifestations of internal atmospheric gravity waves, and an outline of the basic theory is given in Chapter 2.

This theory assumes an isothermal and windless atmosphere in which the effects of viscosity and thermal conductivity are neglected. In practice, however, these effects to play a role in the propagation of the waves. Many authors have added refinements to the theory by assuming more complex models (Pitteway and Hines, 1963, Midgley and Liemohn, 1966, Francis, 1973), but no attempt will be made here to give a comprehensive survey of all the results (see, for example, the review paper by Beer, 1972). Nevertheless, the original, simplified theory remains basically sound.

1.3 Summary

In order to show that the ionosphere has a considerable effect on the direction of arrival of solar radio waves, a series of such measurements was made: at a frequency of 51.7 MHz, solar radio waves were received on both an east-west and a roughly north-south orientation of antenna baseline; at a frequency of 150 MHz with an east-west baseline, both solar signals and satellite signals were analysed, the latter to identify the ionospheric contribution at that frequency. A spectral analysis of the records was made, and the results compared with those predicted in theory.

Chapter 2 of the thesis outlines the theory of the observational technique, a review of basic gravity wave theory, and a discussion of the theory of the focussing of radio waves by a gravity wave induced TID. The third chapter deals with the equipment used, and the analysis

and results are presented in Chapter 4, along with a discussion of the use of the sun as a radio beacon. Chapter 5 contains discussion, conclusions, and suggestions for further work.

CHAPTER 2

THEORY

2.1 Geometrical Considerations

The determination of the angle of arrival of a radio wave at a receiving station is made by measuring the difference in phase of the signals arriving at two antennas separated by a large number of wavelengths. If the antenna separation is d, and the angle of arrival is θ_N, then the path difference is given by $d \cos\theta_N$. See Fig. 2.1. The total phase difference Φ is given by

$$\Phi = 2n\pi + \phi$$

where n is defined below, and $0 \leq \phi < 2\pi$.

Therefore,

$$2n\pi + \phi = \frac{2\pi}{\lambda} d \cos\theta_N$$

and

$$\theta_N = \cos^{-1} \frac{\lambda}{d}(n + \phi/2\pi) \qquad 2.1$$

where λ is the wavelength of the incoming signal, ϕ is the relative phase difference, and n is an integer such that $-\frac{d}{\lambda} \leq n \leq \frac{d}{\lambda}$. It is apparent that there can be a large ambiguity in the determination of θ_N because the exact value of n is unknown. However, one can avoid the problem by choosing n such that the value of θ so determined places the apparent source as close as possible to the centre of the sun.

The geometry used to determine the position of the noise source

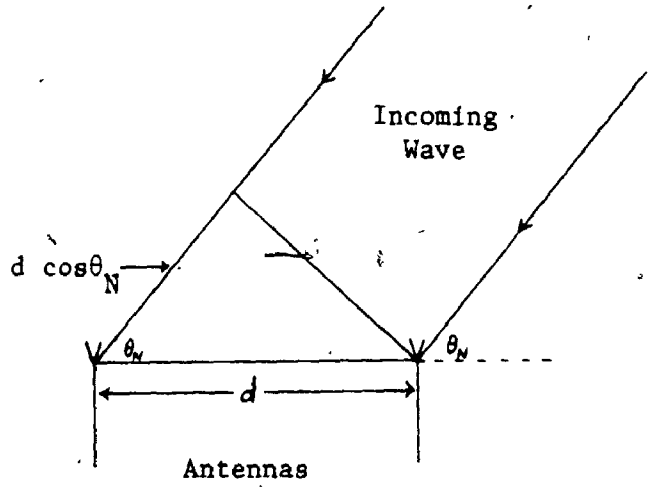

Figure 2.1 Determination of angle of arrival from phase difference at antennas.

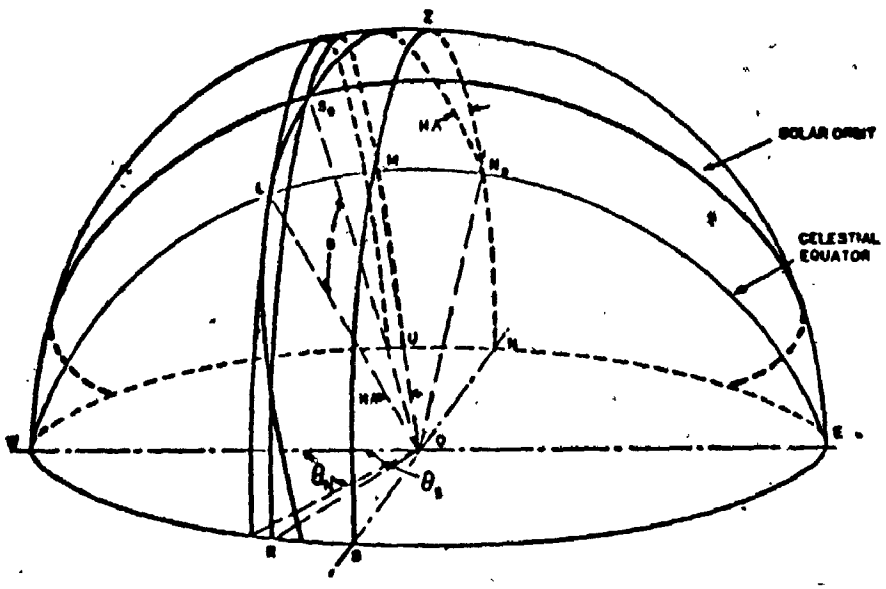

Figure 2.2 Celestial sphere, showing east-west baseline, sun position S_o, and angles θ_S and θ_N.

with respect to the centre of the sun and the baseline of the east-west interferometer is shown in Fig. 2.2 (from Hartz and Hutchison, 1961). The observer is at O and the north celestial pole is at N_p. The location of the centre of the solar disc, S_o, is given by the hour angle HA and the declination D, which can be obtained from the ephemeris of the sun. The azimuthal bearing of S_o with respect to the interferometer baseline is required; in the case of the east-west interferometer, the value of θ_s is to be expressed in terms of HA and D.

From Fig. 2.2 it is seen that the required angle is WOS_o; but it is also WOR since RS_oU is a small circle about the OW axis. In Fig. 2.3 WS_oKE is a great circle passing through the centre of the sun. From the spherical triangle S_oKN_p and the law of sines, we have

$$\frac{\sin(S_oK)}{\sin(KN_pS_o)} = \frac{\sin(S_oN_p)}{\sin(N_pKS_o)}$$

This reduces to

$$\frac{\sin(90°-\theta_s)}{\sin(HA)} = \frac{\sin(90°-D)}{\sin(90°)}$$

which gives

$$\cos(\theta_s) = \sin(HA)\cos(D) \qquad 2.2$$

From equations 2.1 and 2.2 the angle δ_{EW} is defined to be:

$$\delta_{EW} = \theta_s - \theta_N \qquad 2.3$$

This is the parameter referred to as the east-west angle of arrival.

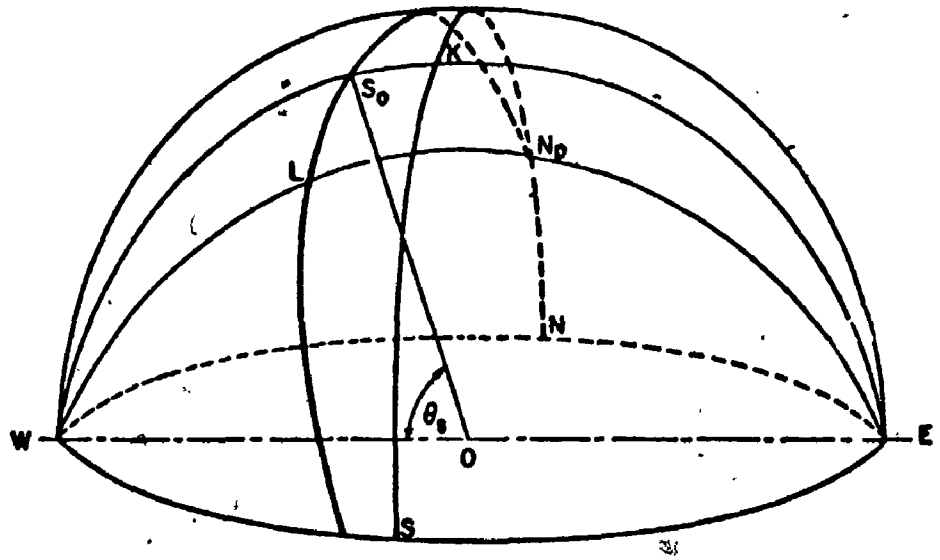

Figure 2.3 The determination of $\cos\theta_S$ from spherical triangle S_oKN_p.

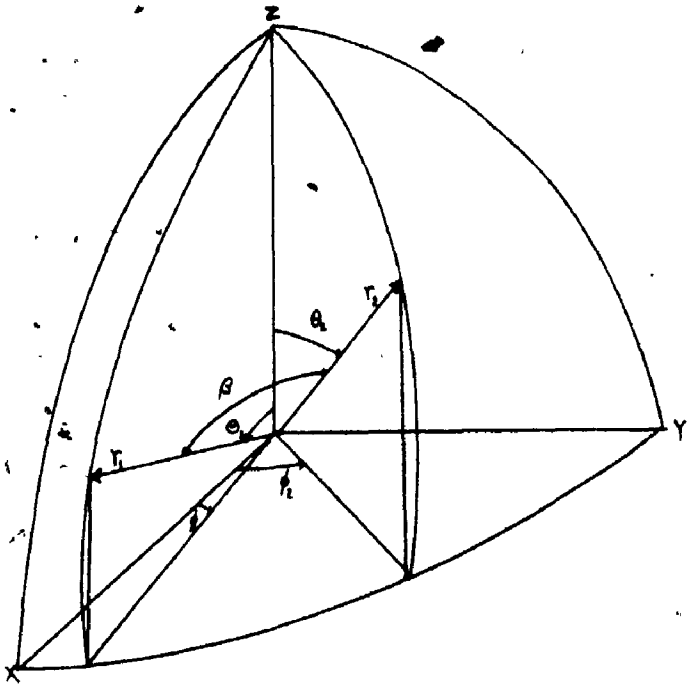

Figure 2.4 Angle between two vectors.

The angle of arrival relative to a north-south baseline can be determined with the aid of similar geometry and the laws of spherical triangles, but it is perhaps useful to look at it in a slightly different way. If two vectors are described in spherical polar coordinates by r_1,θ_1,ϕ_1 and r_2,θ_2,ϕ_2 (Fig. 2.4), then the angle β between them is given by:

$$\cos(\beta) = \cos(\theta_1)\cos(\theta_2) + \sin(\theta_1)\sin(\theta_2)\cos(\phi_1-\phi_2) \qquad 2.4$$

It should be noted at this time that the solar zenith angle χ can be obtained from the following equation (see, for example, Davies, 1965):

$$\cos(\chi) = \sin(\text{lat})\sin(D) + \cos(\text{lat})\cos(D)\cos(HA) \qquad 2.5$$

where lat is the observer's geographical latitude and D and HA are the solar declination and hour angle, as before.

If a coordinate system is arranged so that the Y axis points towards the east and the Z axis points towards the zenith, then equation 2.4 gives the following result for the angle of arrival of a ray from the sun with respect to an east-west baseline:

$$\cos(\theta_S) = \sin(\chi)\sin(\phi_1) \qquad 2.6$$

since $\theta_1 = \chi$, $\theta_2 = \pi/2$, and $\phi_2 = \pi/2$.

Equation 2.6, together with equations 2.2, 2.4, and 2.5, permits the calculation of the angle of arrival of a ray from the sun with respect to a baseline of any orientation. If such an angle is η, and ξ represents the orientation of the antenna baseline with respect to a north-south line, η is defined by:

$$\cos\eta = \cos\psi\cos\xi - \cos\theta_s\sin\xi \qquad 2.7$$

where ψ is the angle of arrival with respect to a north-south baseline and is given by

$$\cos\psi = \sin(D)\cos(lat) - \cos(D)\sin(lat)\cos(HA) \qquad 2.8$$

These equations are easily modified for use with satellite angle of arrival measurements.

2.2 Brief Review of Gravity-Wave Theory

Since a discussion of T.I.D.'s invariably involves gravity waves, it is useful to briefly review the theory which has come to be so widely accepted.

The model developed by Hines (1960) is based on an atmosphere stationary in the absence of waves and uniform in both temperature and composition. Also, superimposed wave motions are assumed to have only perturbation magnitude. Under these assumptions, atmospheric oscillations are governed by the following equations (a detailed discussion of which can be found in Georges, 1967):

$$\rho_o \frac{\partial \vec{U}}{\partial t} = \rho\vec{g} - \nabla P \qquad 2.9$$

$$\frac{\partial P}{\partial t} + \vec{U}\cdot\nabla P_o = C^2\left[\frac{\partial \rho}{\partial t} + \vec{U}\cdot\nabla\rho_o\right] \qquad 2.10$$

$$\frac{\partial \rho}{\partial t} + \vec{U}\cdot\nabla\rho_o + \rho_o\nabla\cdot\vec{U} = 0 \qquad 2.11$$

They represent, respectively, the equation of motion, the equation of adiabatic state, and the continuity equation. $\vec{U}$ is the perturbation

velocity (consisting of the horizontal component, U_x and the vertical component, U_z), P and ρ are the pressure and density (zero subscripts indicate unperturbed values), $\vec{g}$ is the gravitational acceleration, and C is the local speed of sound. If the ratio of specific heats is represented by γ, then C is given by:

$$C^2 = \frac{\gamma P_o}{\rho_o} \qquad 2.12$$

Equations 2.9 and 2.12 can be used to show that

$$P_o,\ \rho_o \propto \exp(-z/H)$$

where H, the neutral atmospheric scale height is given by:

$$H = \frac{C^2}{\gamma g} \qquad 2.13$$

The perturbations in pressure and density are represented by P' and ρ' respectively and are given by:

$$P' = \frac{P-P_o}{P_o} \quad \text{and} \quad \rho' = \frac{\rho-\rho_o}{\rho_o}$$

All perturbation quantities, P', ρ', U_x, U_z are assumed to vary as

$$\exp\ i(\omega t - K_x x - K_z z) \qquad 2.14$$

where ω is the circular frequency of the wave and K_x and K_z are the complex horizontal and vertical wave numbers respectively.

With this last assumption, equations 2.9 - 2.11 yield the following set of four equations:

$$\omega U_x - K_x g H P' = 0 \qquad 2.15$$

$$\rho' g + i\omega U_z - g(1 + iK_z H)P' = 0 \qquad 2.16$$

$$i\omega g H P' - i\omega C^2 \rho' - (g - \frac{C^2}{H})U_z = 0 \qquad 2.17$$

$$i\omega \rho' - iK_x U_x - (\frac{1}{H} + iK_z)U_z = 0 \qquad 2.18$$

For solutions to exist, the determinant of coefficients must vanish, and this leads to the oft-quoted dispersion relation of Hines (1960):

$$\omega^4 - \omega^2 C^2 (K_x^2 + K_z^2) + (\gamma-1) g^2 K_x^2 + i\gamma g \omega^2 K_z = 0 \qquad 2.19$$

As is always pointed out (Hines (1960), Pitteway and Hines (1963), Georges (1967), and others), both K_x and K_z cannot be purely real and non-zero. One assumes $K_x = k_x$ (purely real) and investigates the restrictions on K_z. This assumption for K_x means that appreciable attenuation does not occur over large horizontal distances. It also means that K_z is either purely imaginary, or else

$$K_z = k_z + \frac{i}{2H} \qquad 2.20$$

where k_z is purely real. This leads to the modified dispersion relation:

$$\omega^4 - \omega^2 C^2 (k_x^2 + k_z^2) + (\gamma-1) g^2 k_x^2 - \frac{\gamma^2 g^2 \omega^2}{4C^2} = 0 \qquad 2.21$$

It is the examination of this equation which leads to the conclusion that there are two values for ω (if attention is focussed on positive roots only) associated with each pair of real wave numbers

(k_x, k_z). One of these values of ω must be greater than

$$\omega_a \equiv \frac{\gamma g}{2C} \qquad 2.22$$

and the other must be less than

$$\omega_g \equiv \frac{(\gamma-1)^{\frac{1}{2}} g}{C} \qquad 2.23$$

(Here, ω_g is the same quantity as ω_B, the Brunt frequency, in the notation of Georges, 1967). The values of ω less than ω_g are the ones which are of interest in this study since they form the spectrum of internal atmospheric gravity waves.

The modes of these waves are such that an upward progression of energy is accompanied by a downward progression of phase. Thus the waves travel with a forward tilt in the direction of propagation, the amount of which is determined by the relative values of k_x and k_z. If conditions are such that $k_z^2 \gg \omega_a^2/C^2$, equation 2.21 becomes:

$$\omega^2 k_z^2 \simeq (\omega_g^2 - \omega^2) k_x^2 \qquad 2.24$$

where use has been made of equations 2.22 and 2.23.

Alternatively,

$$(\tau^2 - \tau_g^2)\lambda_z^2 \simeq \tau_g^2 \lambda_x^2 \qquad 2.24(a)$$

where $\lambda_x (\equiv 2\pi/k_x)$ and $\lambda_z (\equiv 2\pi/k_z)$ are the horizontal and vertical wavelengths respectively, and the τ's are the periods corresponding to the respective ω's.

Fig. 2.5 shows the relationship between horizontal and vertical wavelength for a wave travelling with a forward tilt of angle θ_t with the vertical.

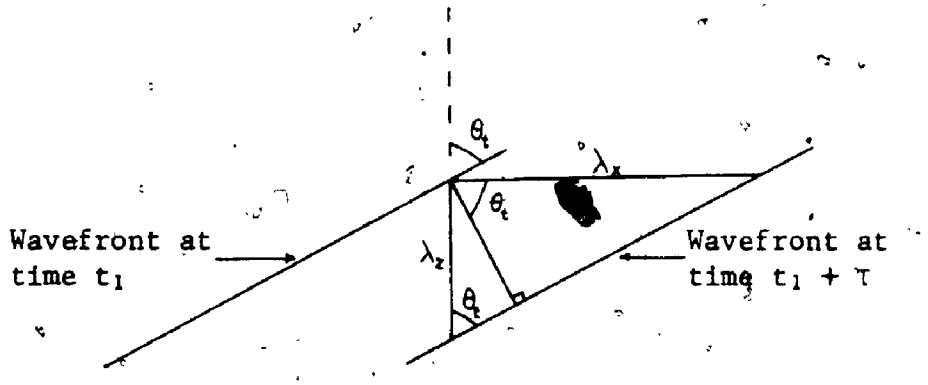

Figure 2.5 Relationship between horizontal and vertical wavelength.

From the diagram,

$$\lambda_z \sin(\theta_t) = \lambda_x \cos(\theta_t)$$

$$\text{or} \qquad \tan(\theta_t) = \frac{\lambda_x}{\lambda_z}$$

From equation 2.24(a)

$$\tau^2 = \tau_g{}^2 (1+\tan^2\theta_t)$$

$$\text{or} \qquad \tau_g/\tau = \cos(\theta_t) \qquad 2.25$$

Hence, for the conditions just outlined, the wavefront tilt can be determined from the period of the wave. The significance of the

wavefront tilt will be discussed further in the next section.

2.3 Gravity Wave Induced Fluctuations in Angle of Arrival Measurements

The focussing of radio waves by ionospheric disturbances plays an important role in angle of arrival measurements. Turnbull and Forsyth (1965) treat the focussing case for isolated irregularities, and Lyon and Holbrook (1972) give a two-dimensional treatment of this effect for the case of travelling ionospheric disturbances and their effect on satellite transmissions. Jones and Lyon (1974) give a three-dimensional treatment as applied to two cases, and it is with one of these cases, the travelling ionospheric disturbance, that this section deals. The discussion here follows essentially from this paper.

The electron density distribution in the ionosphere in the presence of a wave may be expressed as (Georges, 1967):

$$N = N_o \left[1 + a \cos(\omega t - k_x x + k_z z) \exp - \left(\frac{z - z_o}{h} \right)^2 \right] \qquad 2.26$$

where

N = the electron density,

N_o = the unperturbed electron density,

k_x and k_z = the horizontal and vertical wave numbers of the perturbing wave,

ω = the angular frequency of the perturbing wave,

a = the relative amplitude of the perturbing wave,

z_o = the height of maximum amplitude of the

perturbing wave,

h = the height above and below z_o at which the amplitude of the perturbing wave falls off by a factor of 1/e.

The projection of k_x on the surface of the earth defines the x direction. The model is intended to approximate an increase in wave amplitude with height to a certain value, followed by a damping process (eg. viscous damping, Pitteway and Hines, 1963).

The refractive index of the medium, μ, is given approximately by:

$$\mu = 1 - \frac{KN}{f_o^2} \qquad 2.27$$

where f_o is the radio wave frequency and K is a constant, equal to 40.3 in MKS units. Hence, the phase path difference, Δp, from the free space value is given by

$$\Delta p = - \frac{K}{f_o^2} \int N dv \qquad 2.28$$

where v is measured along the ray path.

In order to evaluate this expression, it is convenient to express N in terms of a coordinate system u,v,w such that v is in the direction of the ray path and w is in the x-y plane. The origin of the new coordinate system is the point in the ionosphere where the line joining the observer and the source passes through the height level z_o. The relationship between the coordinate systems is as follows:

$$x = - u \sin(e)\cos(\zeta) + v \cos(e)\cos(\zeta) - w \sin(\zeta) + z_o \cot(e)\cos(\zeta)$$

$$y = - u \sin(e)\sin(\zeta) + v \cos(e)\sin(\zeta) + w \cos(\zeta) + z_o \cot(e)\sin(\zeta)$$

$$z = u \cos(e) + v \sin(e) + z_o \qquad 2.29$$

where e is the elevation angle and ζ is the angle between the azimuth of look and the x-axis.

Only the perturbation part, p' of equation 2.28 will be considered since the term representing the total electron content will disappear later on differentiation. Since the change in this parameter occurs slowly with respect to the length of a wave period, the assumption of constant total electron content will not severely restrict the discussion. Hence, from equation 2.26:

$$p' = - \frac{K}{f_o^2} aN_o \int \cos\left[\omega t - k_x(-u \sin(e)\cos(\zeta) + v \cos(e)\cos(\zeta) - w \sin(\zeta) + z_o \cot(e)\cos(\zeta)) + k_z(u \cos(e) + v \sin(e) + z_o)\right] \exp\left[- \frac{(u \cos(e) + v \sin(e))^2}{h^2} \right] dv \qquad 2.30$$

If $z_o >> h$, the integration may be taken from $-\infty$ to $+\infty$ with negligible error, so that:

$$p' = \frac{- KaN_o h \sqrt{\pi}}{f_o^2 \omega \sin(e)} \cos\left[\omega t + u k_x \frac{\cos(\zeta)}{\sin(e)} + w k_x \sin(\zeta) + z_o(k_z - k_x \cot(e)\cos(\zeta))\right] \exp\left[- \frac{h^2}{4}(k_z - k_x \cot(e)\cos(\zeta))^2 \right] \qquad 2.31$$

The angular deviation, $\theta(1)$, is found by evaluating:

$$\theta(\hat{1}) = \nabla p' \cdot \hat{1} \qquad 2.32$$

where $\hat{1}$ is a coordinate (unit vector) with respect to which the angular deviation is measured, and the evaluation is to take place at the origin of the u,v,w coordinate system. In order to be detected by an interferometer, the angular variations must be in a plane normal to the line of sight, and also in the plane defined by the interferometer baseline and the line of sight. Thus, $\nabla p'$ is in the u-w plane, $\hat{1}$ is in the u-w plane and also in the plane defined by the line of sight (v) and the axis of the interferometer. The orientation of $\hat{1}$ is determined by evaluating $(\hat{v} \times \hat{y}) \times \hat{v}$ and normalizing the resulting direction cosines by ensuring that $\hat{1}_u^2 + \hat{1}_v^2 + \hat{1}_w^2 = 1$. Equation 2.29 can easily be made to represent a fixed coordinate system (ie, x = south, y = east, z = vertical) by substituting ϕ (azimuth of line of sight) for ζ(line of sight from wave propagation direction). Hence, $\zeta = \phi - \alpha$, where α is the direction of wave propagation measured with respect to the fixed x (south) axis. The components of $\hat{1}$ in the u,v,w, coordinate system are:

$$\hat{1}_u = -\sin(e)\sin\phi/(\sin^2(e)\sin^2(\phi) + \cos^2(\phi))^{1/2}$$

$$\hat{1}_v = o$$

$$\hat{1}_w = \cos\phi/(\sin^2(e)\sin^2(\phi) + \cos^2(\phi))^{1/2} \qquad 2.33$$

The resulting angular variation with respect to an east-west baseline is:

$$\theta_{EW} = \frac{\partial p'}{\partial u}\,\hat{1}_u + \frac{\partial p'}{\partial w}\,\hat{1}_w \Big|_{u,v,w = o}$$

$$= - \frac{KaN_o\, h\, \sqrt{\pi}}{f_o^2 \sin(e)} \exp\left[- \frac{h^2}{4} \left(k_z - k_x \cot(e)\cos(\phi-\alpha) \right)^2 \right]$$

$$\frac{k_x \sin\alpha}{\left(\sin^2(e)\sin^2(\phi) + \cos^2(\phi) \right)^{1/2}} \cos\left[\omega t + z_o (k_z - k_x \cot(e)\cos(\phi-\alpha)) \right] \qquad 2.34$$

In a manner similar to that just outlined, the angle of arrival with respect to a north-south baseline can be determined (in the present study, the north-south antenna baseline was actually oriented 17.74° (0.3096 rad) east of the fixed south axis, accounting for the number 0.3096 in the following equation):

$$\theta_{NS} = - \frac{KaN_o\, h\, \sqrt{\pi}}{f_o^2 \sin(e)} \exp\left[- \frac{h^2}{4} \left(k_z - k_x \cot(e)\cos(\phi-\alpha) \right)^2 \right]$$

$$\frac{k_z \cos(\phi-0.3096)}{\left(\sin^2(e)\cos^2(\phi-.3096) + \sin^2(\phi-0.3096) \right)^{1/2}} \cos\left[\omega t + z_o (k_z - k_x \right.$$

$$\left. \cot(e)\cos(\phi-\alpha) \right] \qquad 2.35$$

Examination of equations 2.34 and 2.35 reveals some important points. If a wave is travelling directly south, for example, the sin (α) term in equation 2.34 shows that there will be no angular variations observed with respect to an east-west baseline. A similar result holds with east-west travelling waves and a north-south baseline. The wavefront tilt (determined by the relative values of k_x and k_z) plays an important role in the observation of angular variations. The largest variations will be detected when the line of sight closely aligns with the wavefront tilt. Because of the time variation of the angles of elevation and azimuth, the observed

frequency may be significantly different from the actual wave frequency. Since the principal difference between equations 2.34 and 2.35 lies in the sinusoidal term involving α, it follows that amplitude ratios determined from readings from two baseline orientations will yield the direction of travel of the perturbing wave. (The different normalization factors in equations 2.34 and 2.35 are known, slowly-varying functions of time, and can be taken into account in actual calculations.)

2.4 Correlation

It is frequently useful to investigate the general dependence of the values of one set of data on the values of another at various intervals along the time axis. This is termed cross-correlation; if the two functions are one and the same, the procedure is termed autocorrelation. Correlation for finite, discrete data is presented in the form of correlation coefficient versus lag number (time shift). The correlation coefficient can vary from +1 if the function is exactly duplicated at this lag, to zero if there is no correlation, and to -1 if the functions exactly cancel each other out. For example, a sine curve is in phase with itself once every cycle, and 180° out of phase once every cycle, so the autocorrelation function is a cosine curve with amplitude 1.

The autocorrelation function is given by:

$$R(L) = \frac{1}{R_o} \frac{1}{n-L} \sum_{i=1}^{n-L} X_i X_{i+L} \qquad 2.36$$

where R(L) is the correlation coefficient at lag L, n is the number of points in the record, and the X_i are the data points in the record.

R_o is the normalizing term found by knowing that the autocorrelation coefficient is unity at zero lag. Hence,

$$R_o = \frac{1}{n} \sum_{i=1}^{n} X_i^2 \qquad 2.37$$

The cross-correlation between two functions X and Y is given by:

$$R_{XY}(L) = \frac{1}{\sqrt{R_{XO}}} \frac{1}{\sqrt{R_{YO}}} \frac{1}{n-L} \sum_{i=1}^{n-L} X_i Y_{i+L} \qquad 2.38$$

where $R_{XY}(L)$ is the cross-correlation coefficient at lag L, R_{XO} and R_{YO} are found for functions X and Y using equation 2.37.

CHAPTER 3

EQUIPMENT

The equipment used in this experiment consisted principally of two sections. The observations at 51.7 MHz were made with a phase-swept interferometer designed and constructed at the Defence Research Telecommunications Establishment (now the Communications Research Centre) at Shirley Bay, near Ottawa. The observations at 150 MHz were made using a phase measurement receiving system originally designed for use at 40 MHz and converted for use at the higher frequency.

3.1 Angle of Arrival Measurements at 51.7 MHz Using a Phase-Swept Interferometer.

A phase-swept interferometer works basically on the following principle (Little and Payne-Scott, 1951, Winacott, 1961). Consider a signal of the form

$$A \sin(\omega t) \qquad 3.1$$

arriving at a receiver from one antenna of a widely separated pair, where A is the amplitude, ω is the angular frequency, and t is the time. If the antennas and transmission lines are identical, then the signal arriving from the other antenna can be represented as

$$A \sin(\omega t + \Phi) \qquad 3.2$$

where Φ is the total phase difference between the signals arriving at the

two antennas. The phase of this signal can be artificially swept at a rate ω_s and so the signal from the second antenna can now be represented as

$$A \sin(\omega t + 2n\pi + \phi + \omega_s t) \qquad 3.3$$

where the expanded expression for Φ (from Chapter 2) has been used. If the signals are now added together, the output has the form

$$2A \sin\left[\omega t + \frac{2n\pi + \phi + \omega_s t}{2}\right] \cos\left[\frac{2n\pi + \phi + \omega_s t}{2}\right] \qquad 3.4$$

In this expression, the sin term is completely dominated by the R.F. term ωt, since ω represents a frequency of the order of MHz, and ω_s is of the order of just a few Hz. The cosine term, on the other hand, represents a modulation of the amplitude of the R.F. signal, so that the sinusoidal term involving $\omega_s t$ and ϕ can be extracted from the detected modulation envelope by a narrow band-pass filter. This can be compared in a phase meter with a reference signal (of the form $\cos(\omega_s t)$) generated by the phase shifter. Thus, the relative phase difference, ϕ, between signals arriving at two separated antennas can be determined. The discussion applies equally well, whether the phase shifter is inserted into the actual R.F. signal path or into one arm of a local oscillator output in the process of heterodyning the signals.

A detailed description of the 51.7 MHz interferometer system is given by Winacott(1963) and won't be repeated here. In the actual configuration used, there were two interferometers, one using an east-west antenna baseline, the other an approximate north-south baseline, with one antenna common to both orientations. The relative phase was

continuously recorded on paper chart recorders, onto which time marks, triggered by an accurate digital read-out clock, were placed every ten minutes.

3.2 Phase Measurements at 150 MHz

The receiving system used for the 150 MHz measurements was designed to operate on the phase measurement principle used in the U.S. Navy Minitrack satellite tracking stations. The relative phase between the signals received at the antennas is maintained throughout the system by preserving their instantaneous frequency difference. A detailed description of the receiving system is given by Dixon and Livingstone (1969), and only a brief outline will be given here.

Since the system was designed for 40 MHz, signals at 150 MHz were converted to the lower frequency using converters operating from a common local oscillator. The signals were then fed into the separate front ends of the 40 MHz system. The first I.F. was approximately 11.3 MHz for both signals, but they differed from each other by 500 Hz because of the difference in frequency of the first two local oscillators. The 500 Hz difference frequency between these oscillators was phase-locked with the 500 Hz precision frequency standard, called the reference signal. The relative phase of the 500 Hz difference in I.F.'s with respect to the 500 Hz reference was determined by the relative phase difference existing between the signals at the two antennas.

The 11.3 MHz signals were heterodyned once more using a common oscillator to preserve the instantaneous frequency difference, and the final I.F.'s were 455.5 KHz and 456 KHz. The 500 Hz difference between these signals was detected and compared in a phase meter with the 500 Hz reference signal. This relative phase difference was

continuously recorded on a chart recorder and was due to the phase difference between the signals at the two antennas. As with the 51.7 MHz interferometer, time marks were placed on the charts every ten minutes. Since the system was designed for use with satellite transmissions, all necessary information, including a time signal such as the IRIG"C" code, could easily be placed on magnetic tape, and the useful information extracted at a later date.

CHAPTER 4

ANALYSIS AND RESULTS

4.1 Analysis Considerations

As indicated in Chapter 3, the output from the phase meters was placed on Esterline Angus chart recorders. The chart speed for the 51.7 MHz phase records was 24 inches per hour and for the 150 MHz records, it was 45 inches per hour. The charts were scaled with the aid of a Gerber scaler which is capable of digital readouts to the nearest 0.01 inches. The 51.7 MHz charts were sampled at a rate of 96 times per hour and the 150 MHz records at 180 times per hour. The relative angle of arrival values were computed using equations 2.1, 2.2 and 2.3. As mentioned in Chapter 2, there is always an ambiguity in the absolute value of the angle of arrival because of the term n in equation 2.1. However, for relative values this is unimportant, and n was always chosen such that the absolute value of δ was a minimum, ie, θ_N closest in value to θ_S. Figs 4.1 and 4.2 show sample records of relative angle of arrival versus time.

In order to investigate the presence of dominant periods, the records were further analysed with the aid of a fast Fourier transform computer subroutine. The Fourier transform is simply a method of looking at data in a more convenient form. In this case, instead of looking at the amplitude versus time records, the transform allows the observation of different amplitudes at different frequencies

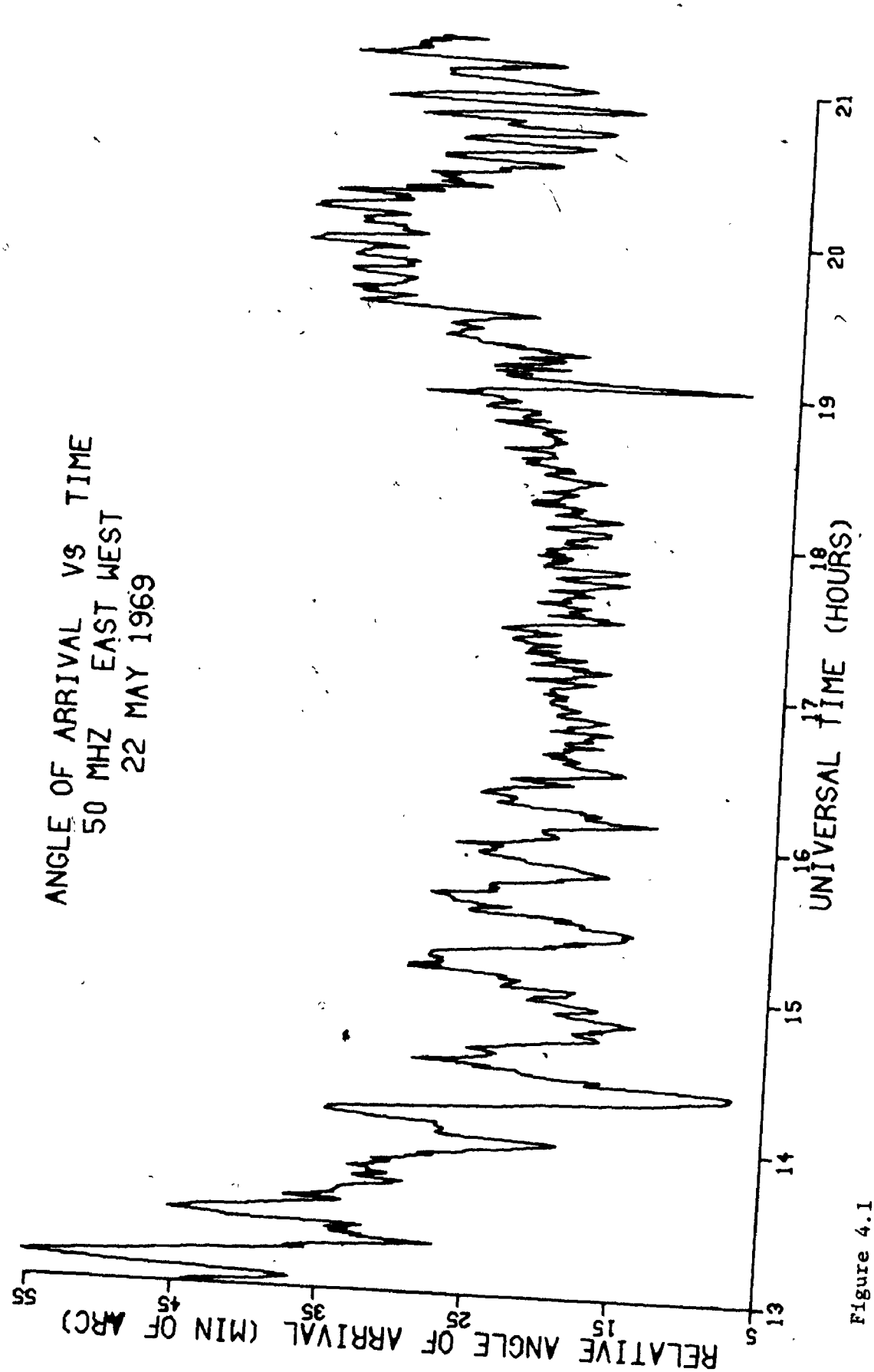
ANGLE OF ARRIVAL VS TIME
50 MHZ EAST WEST
22 MAY 1969
RELATIVE ANGLE OF ARRIVAL (MIN OF ARC)
55
45
35
25
15
5
13
14
15
16
17
18
19
20
21
UNIVERSAL TIME (HOURS)

Figure 4.1

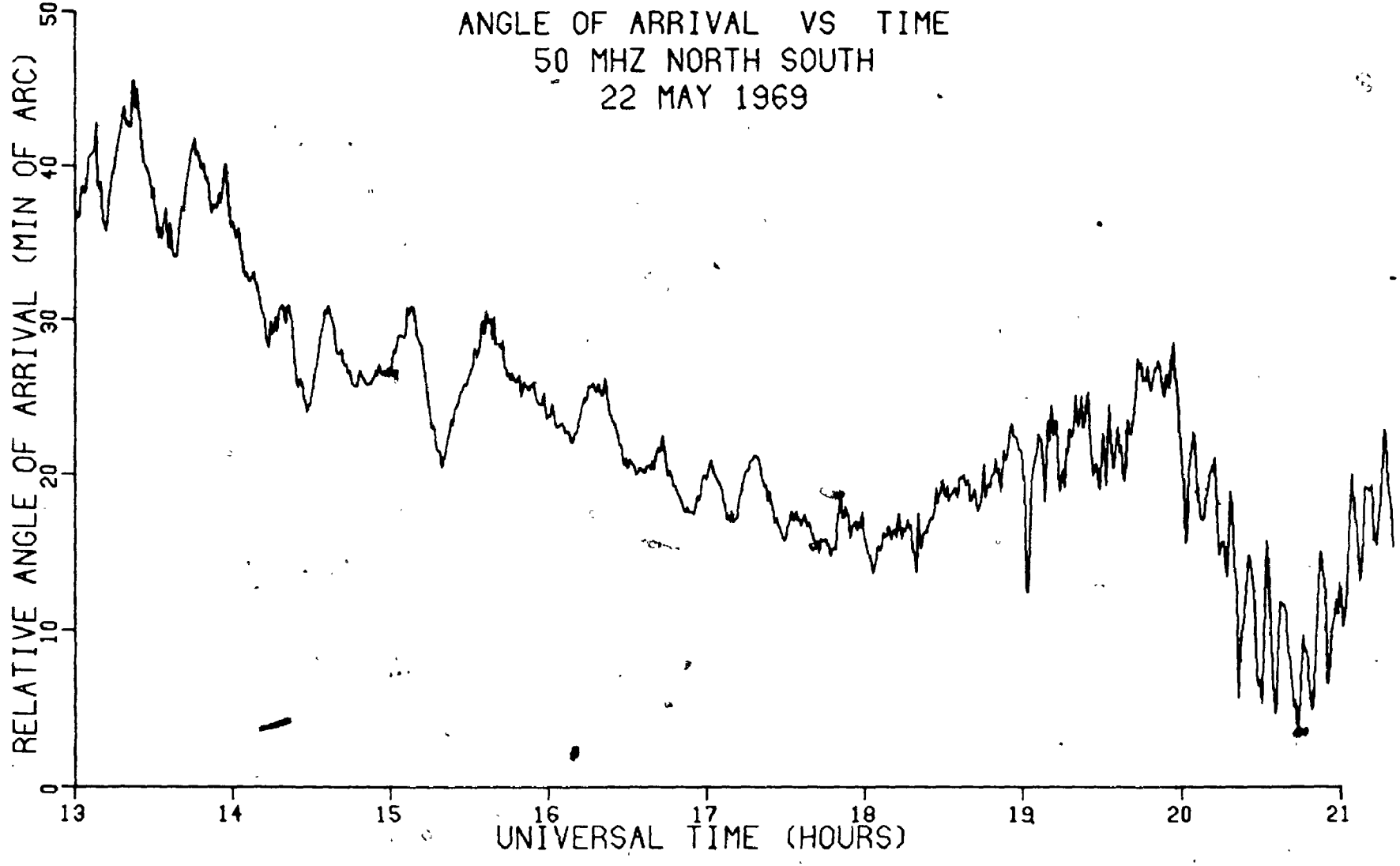
ANGLE OF ARRIVAL VS TIME
50 MHZ NORTH SOUTH
22 MAY 1969
RELATIVE ANGLE OF ARRIVAL (MIN OF ARC)
0
10
20
30
40
50
13
14
15
16
17
18
19
20
21
UNIVERSAL TIME (HOURS)

Figure 4.2

(or periods). The first three or four hours of data in Fig. 4.1 indicates, on a visual inspection, a fairly dominant period around 23 minutes, but, as will be shown later, the Fourier transform shows much more than is readily seen on first glance.

The original algorithm for the fast Fourier transform (or FFT as it is frequently called) was developed by J.W. Cooley and J.W. Tukey (Cooley and Tukey, 1965) and a great many particular programs have been written since their work first appeared. The program used in the present analysis was taken from one written by Michael Foreman (Foreman, 1966) and adapted by G. Otis at Universite Laval. The principal advantage of the FFT over other methods is the vast saving in computer time; this saving is by a factor of $N/\log_2 N$ where N is the number of points for which the transform is calculated. (See, for example, Gentlemen and Sande, 1966, or A.J. Villasenor, 1968). If a 2048 point transform is performed on that number of data points, then the FFT method is faster than other methods by a factor of 2048/11, or almost 200.

There should be noted at this time some of the procedures used to treat the angle of arrival data before the Fourier transform is applied. If there is a pure sine wave and a record of infinite length, the transform will be a delta function at the frequency of the wave. However, only finite record lengths are available, and so the output from the transform will be a broader spectral line, centered at the wave frequency, but with side lobes, since the transformed record is of the form sin (x)/x. A number of spectral windows have been developed to apodize, or remove side lobes, from spectra. The particular one used in this analysis was the Connes apodizing function, and reduced

the first (and hence, the highest) side lobe by a factor of five at the expense of broadening the spectral line by about fifty per cent (this measurement taken at one half the maximum amplitude of the line). This apodization routine also reduced the amplitude of the spectral line by a factor of 8/15, but this is easily taken into account.

Apodization, of course, does not eliminate all problems. If there are two spectral components close together, side lobes can lead to false information about the true amplitude of one or both waves. If the records are apodized, then the broadening of one spectral line could possibly totally mask a small peak close by. These considerations tend to add a small degree of uncertainty to the actual values of amplitude and frequency, and reasonable estimates of probable errors must be made.

Another consideration which must be taken into account is that of slow trends. This can be envisaged as one or more sine components superimposed on a line of constant slope. If some method is not used to get rid of the trend, it will appear, on the FFT output, as a very large, very long period wave which could effectively obscure the very waves desired for observation. The method of trend removal used in this analysis was that of the running mean. (See Webster, 1972). A length of record is averaged, the result subtracted from the value at the mid-point of the section of data, and the process repeated, moving from one end of the record to the other. It is obvious that a certain number of the total number of points in the section of record under consideration will be lost, but this can be tolerated in view of the necessity for the removal of the trend. The length of time over which the running mean is taken must be at least as long as the

periods under investigation.

The effect of this type of trend removal is different for the different frequencies involved, but it is possible to calculate how much each frequency has been affected and to compensate accordingly.

The effect of noise must also be considered. Here, noise is simply a term used to describe variations in the signal due to any of a number of possible causes, other than well-defined ionospheric wave motion. Such possible causes include data scaling errors, isolated ionospheric irregularities not associated with large-scale wave motion, and rapid changes in the angle of arrival caused by sources in the atmosphere of the sun itself. These factors can all affect, to a certain degree, the frequency spectra from the Fourier transform.

Appendix A contains a discussion of the uncertainties involved in reducing the phase information to relative angle of arrival values, and for the 50 MHz records, 0.5 minutes of arc is the associated error. The amplitude of noise on the output from the FFT is considerably less than the estimate of the error of individual input values because the noise level is smeared throughout the entire record. For typical record lengths and transform lengths used in this study, an uncertainty of 0.5 min. of arc in an individual input data point represents only 0.03 min. of arc on the output amplitude. Thus the scaling of the data contributes negligible error to the FFT output.

The angle of arrival from the interferometer is that derived from the average of the signal received at the antennas from the source on the sun. However, the size of such sources is generally of the order of 10 minutes of arc and strong radio bursts from an area other than the principal source centre appear on angle of arrival records.

Dramatic evidence of this can be seen just after 1900 UT in Figs 4.1 and 4.2. The time of occurrence of the large data spike exactly coincides with the time of a large group of Type III radio bursts from the sun. This particular group of bursts caused a change of 15 minutes of arc on the east-west record, and somewhat less on the north-south interferometer. The burst-like nature of the sun's radio emission is certain to cause angle of arrival fluctuations of a few minutes of arc, and so, along with isolated ionospheric irregularities, it must be considered as a source of noise since the specific identification of such events is not always possible.

4.2 Angle of Arrival Measurements from the Sun

4.2.1 Results Predicted from Theory

According to equation 2.34 derived in Chapter 2, the observed frequency and amplitude of relative angle of arrival measurements disturbed by atmospheric gravity waves will vary throughout the day because of the change in aximuth and elevation of the "look" vector. If the following ionospheric and wave parameters are adopted, the theoretical variations in the angle of arrival of a signal arriving from the sun can be evaluated. The position parameters for the sun were taken for 22 May, 1969.

h	= 50 km	a	= 0.1
f_o	= 51.7 MHz	N_o	= 5×10^{11} m^{-3}
λ_x	= 100 km	λ_z	= 100 km
z_o	= 300 km	Period	= 21 min
Azimuth	= 75° E of S		

The results of the calculation are shown in Fig. 4.3. It can be seen that the amplitude of the variations increases to a maximum, and then decreases with increasing time, during which the frequency (and hence, period) is also changing. The maximum variation occurs around 1400 UT. At that time the solar zenith angle was 47° and the look azimuth was 78°. Since the wavefront tilt was 45° and the propagation azimuth was 75°, it is seen that a great enhancement in variations occurs when the line of sight closely aligns with both the direction of wave propagation and the wavefront tilt. If the first four hours of the simulated record are analysed with the FFT, the period is found to be 15.8 minutes, significantly different from 21 minutes, the period of the wave. The 15.8 minute period is, of course, not exact, since the period is continuously changing throughout the record. This is one aspect which tends to broaden the spectral lines as determined by the FFT analysis. If another four hour section of the stimulated record is analysed, but this time from 1400 to 1800 UT, the period is apparently 16.4 minutes, measureably different from 15.8 minutes, and still significantly different from the wave period of 21 minutes. Also, the amplitude of the peak according to the FFT analysis has decreased from 19.2 to 9.8 minutes of arc. (Strictly speaking, the dimensions of the FFT output are those of amplitude times time.)

If a change is made in just one of the parameters listed above, namely the direction of propagation, significantly different results are predicted. Fig. 4.4 is a graph similar to that of Fig. 4.3, except that the direction of propagation of the wave is 30 degrees west of south. For the same time of day as the first wave, the actual

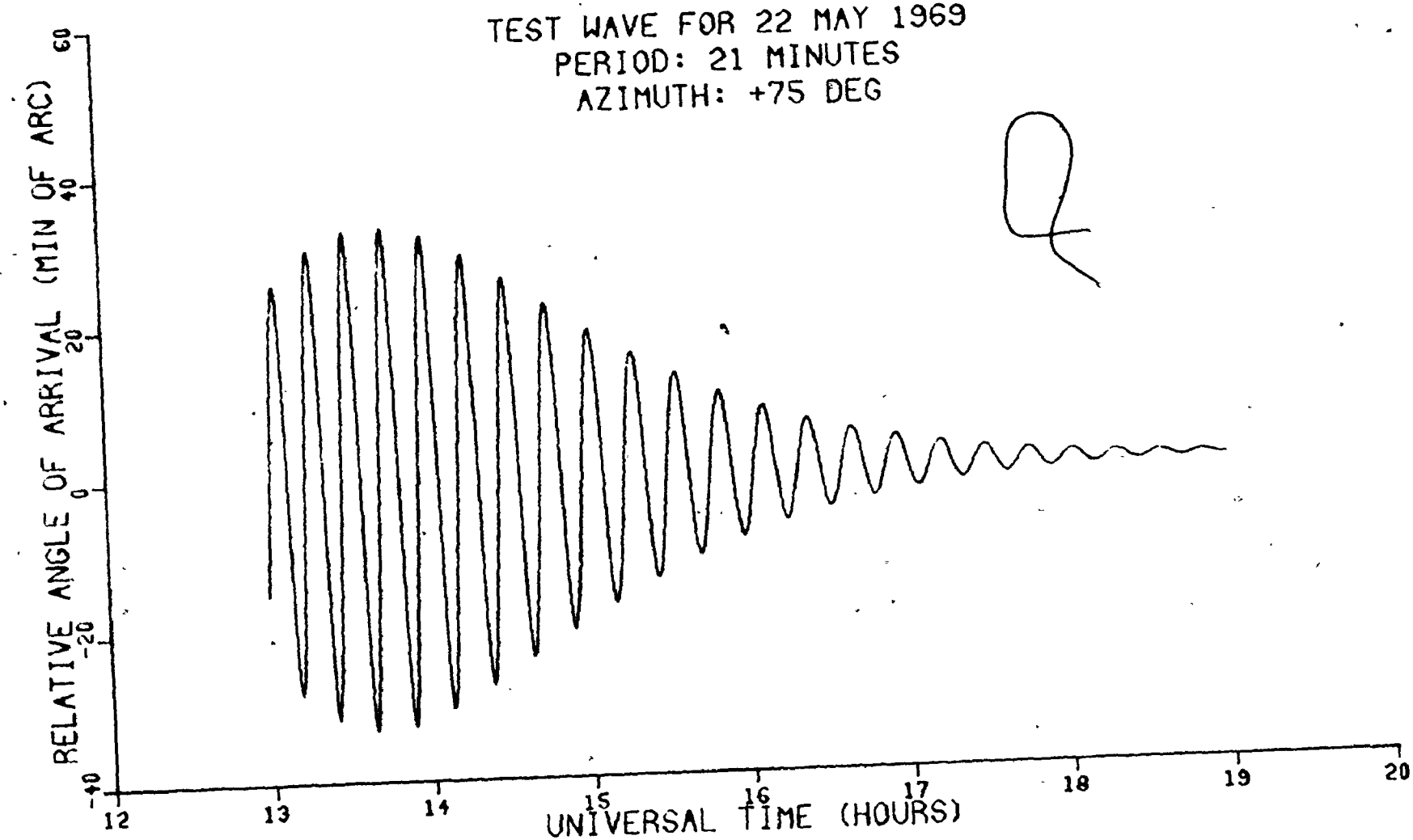
TEST WAVE FOR 22 MAY 1969
PERIOD: 21 MINUTES
AZIMUTH: +75 DEG
RELATIVE ANGLE OF ARRIVAL (MIN OF ARC)
60
40
20
0
-20
-40
12
13
14
15
16
17
18
19
20
UNIVERSAL TIME (HOURS)

Figure 4.3

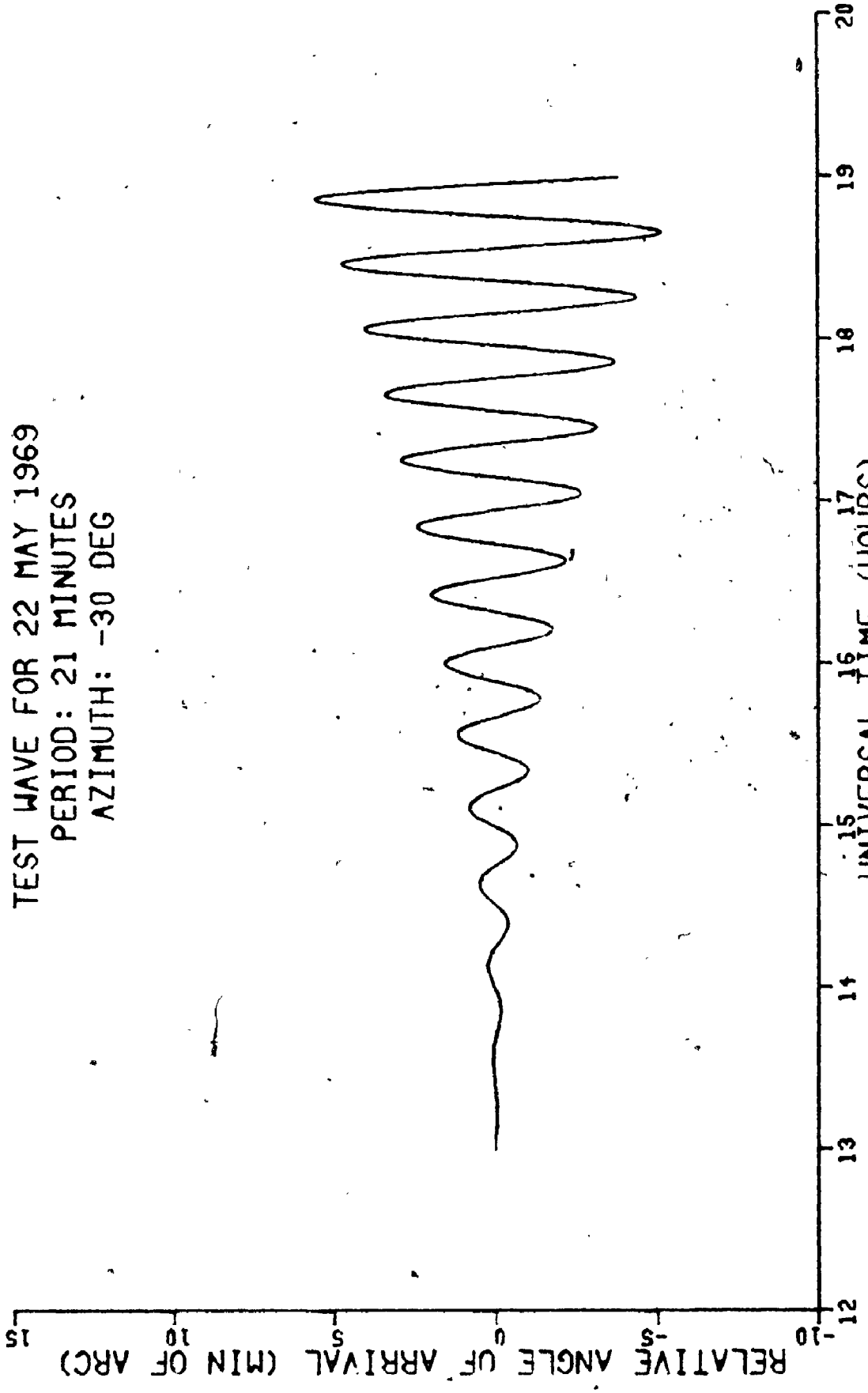
TEST WAVE FOR 22 MAY 1969
PERIOD: 21 MINUTES
AZIMUTH: -30 DEG
RELATIVE ANGLE OF ARRIVAL (MIN OF ARC)
15
10
5
0
-5
-10
12
13
14
15
16
17
18
19
20
UNIVERSAL TIME (HOURS)

Figure 4.4

value of the variation is considerably less, starting at essentially zero and increasing in amplitude as the day progresses. In this case, the line of sight did not align with both the wavefront tilt and direction of propagation at the same time and it is seen that the maximum amplitude was not attained during the observation period. The FFT analysis in this case gives an amplitude of 0.8 minutes of arc at a period of 27.2 minutes for the first four hours of the record, and 1.6 minutes of arc at a period of 25.6 minutes for the section of record from 1400 to 1800 UT. Again, these periods are noticeably different from the actual wave period of 21 minutes.

This test procedure was repeated for a wave using somewhat different parameters, and the results for all three are presented in Table 4.1. These theoretical results are for single waves and angles of arrival measured with respect to an east-west baseline at an observation frequency of 51.7 MHz. Equations 2.34 and 2.35 show that measurements with respect to the north-south baseline will differ only because of the sinusoidal term of α, the direction of wave propagation, and the slowly-varying normalization factors. Observations at a higher frequency differ only in the $1/f_o^2$ dependence. However, these three examples show clearly how the amplitude of variations and apparent wave frequency change significantly during the time of observation.

Cross-correlation coefficients for pairs of records (east-west and north-south baseline orientations) would be +1 at zero lag for the single wave cases just outlined. However, this would not generally be realized in practice, and in order to obtain a more realistic picture, two further factors were considered. First, a number of waves of

TABLE 4.1

Test Wave Analysis Summary

h = 50 km; a = 0.1; $\lambda_x = \lambda_z$ = 100 km; f_o = 51.7 MHz

N_o (m^{-3})	z_o (km)	Period (minutes)	Azimuth (Deg E of S)	Time of Record (UT, hours)	Obs. Period (minutes)	Obs. Amp. (min of arc)
5×10^{11}	300	21	+75	1300 - 1700	15.8	19.2
				1400 - 1800	16.4	9.8
5×10^{11}	300	21	-30	1300 - 1700	27.2	0.8
				1400 - 1800	25.6	1.6
2.5×10^{11}	200	15	+75	1300 - 1700	12.9	9.5
				1400 - 1800	13.2	4.8

different parameters were included instead of only one, and secondly, a noise level was simulated for the test data. This noise level was added using random numbers, assuming that the uncertainties in the evaluation of the angle of arrival represent white noise.

Theoretically, two sets of random numbers will give a cross-correlation function that is everywhere zero, but small sample sizes mean that this is not generally the case. It was found that the random numbers (strictly speaking, pseudorandom numbers generated by computer) used in these test procedures never gave correlation coefficients greater than 0.12. This was also true when a set of random numbers was correlated with a test signal such as that of Fig. 4.3.

Since Figs 4.1 and 4.2 indicate that a number of periodic disturbances are present, sets of test data were prepared by adding the contributions from up to six waves with different periods, wavelengths, directions of propagation, and heights of maximum effect. The parameters were chosen to be consistent with observations of travelling ionospheric disturbances reported in the literature. The cross-correlation functions for the east-west and north-south data were calculated and all sets of test data were analysed with the fast Fourier transform.

Generally, the test results showed correlation coefficients from 0.5 to 0.8 and emphasized the system's sensitivity to the geometry involved. The waves with large eastward components of motion were easily detected early in the day when the observation of westward travelling waves was suppressed. Later in the day, the reverse was true. The possibility of a very real problem in interpretation became

evident. As previously explained, waves with eastward components of motion will be observed to have periods shorter than the true wave period, and westward travelling waves will cause periods to appear longer. If the two shifted periods are close in value, interpretational difficulties will arise.

The test results indicate that the amplitudes from the east-west and north-south data from the FFT analysis can be used to determine the direction of wave travel, as suggested in Chapter 2. (The ratio of amplitudes should give the tangent of the direction of propagation, subject to a slowly-varying normalization factor and a slight modification to allow for the north-south baseline being 17.74° away from true north-south.) The method is more reliable for waves travelling southeast or southwest, and tends to break down when the observed effect of the wave decreases significantly, as in the case of a wave travelling normal to one of the antenna baselines.

4.2.2 Experimental Results

Comparison of the test data of Figs. 4.3 and 4.4 with the experimental data of Fig. 4.1 shows clearly that there is something considerably more complicated than a single, pure gravity wave changing the relative angle of arrival of the signal in exactly the manner described by equation 2.34. However, Georges (1968) has suggested that the ionosphere can support a large number of superposed gravity waves propagating upward from below; the higher frequency waves being progressively damped out by viscous effects described first by Pitteway and Hines (1963). Since the radio signal from the sun traverses the entire ionosphere, the observed results at the

receiver will be the combination of all perturbations occurring throughout the whole path. So even though observations of F region gravity waves of periods less than about 15 minutes are not expected, disturbances in the E region could manifest themselves as characteristic periods as low as eight or nine minutes. The change in period due to the motion of the sun through the ionosphere can contribute to still shorter periods being observed if the disturbances have an eastward component of travel.

Fig. 4.2 shows the relative angle of arrival versus time for the same day as the data of Fig. 4.1, but for the (approximately) north-south oriented interferometer. These two graphs strongly indicate periodic variations at a number of characteristic frequencies. In using the fast Fourier transform to analyse the results, sections of record four hours long were selected, with the starting time of each successive section advanced by one hour. This way, it should be apparent if a particular wave varies in amplitude and/or frequency. However, difficulties can still arise. The FFT gives a measure of the presence of a particular spectral component during the entire length of record. So a given wave might have a certain amplitude for only two hours, and then die out, but on the FFT output, it would appear to have a smaller amplitude because of the longer record length. Also, it is not always easy to see exactly when the contribution of a particular wave starts or stops. This makes quantitative studies of amplitude variations very difficult. Since the large data spike at 1900 UT was identified as a group of Type III radio bursts from the sun, it was deleted from the records before the spectral analysis was performed. Its appearance on the frequency record would

be a sinusoidal variation, and as such, could seriously affect the amplitudes of other spectral peaks.

Theoretically, waves detected on both east-west and north-south baselines will be in phase or 180° out of phase. This should enable the determination of the quadrant of the direction of propagation of the wave to be made. This determination can also be made because of the high degree of sensitivity of the method of observation to the azimuth of the line of sight, and the lack of good phase information (because of large phase fluctuations from the spectral analysis) was not a problem in this study.

Figs. 4.5 to 4.14 are the transformed outputs for the records of Figs. 4.1 and 4.2. The graphs are presented so that the record from the north-south interferometer immediately follows that of the east-west interferometer for the same time of day. The amplitudes are all normalized so that the largest peak has an amplitude of unity, and the scale factor given is the factor by which the values in the graph must be multiplied in order to give the true amplitude as given by the FFT. For example, in Fig. 4.5, the scale factor is 4.29, so that the amplitude of the highest peak is 4.29 minutes of arc.

The changes in the spectra can be followed by study of Figs. 4.5 through 4.14. Fig. 4.5 shows two strong peaks, one with a period of just over 30 minutes (frequency 1.97 c/hr), and one at 21 minutes (2.84 c/hr). The north-south record for the same time of day exhibits a double peak centered around 30 minutes, and a smaller peak at 16.6 minutes (3.61 c/hr). For the sections of the records between 1400 and 1800 UT, the scale factors have decreased in both cases; the 21 minute period has become dominant in the east-west record, and the double peak

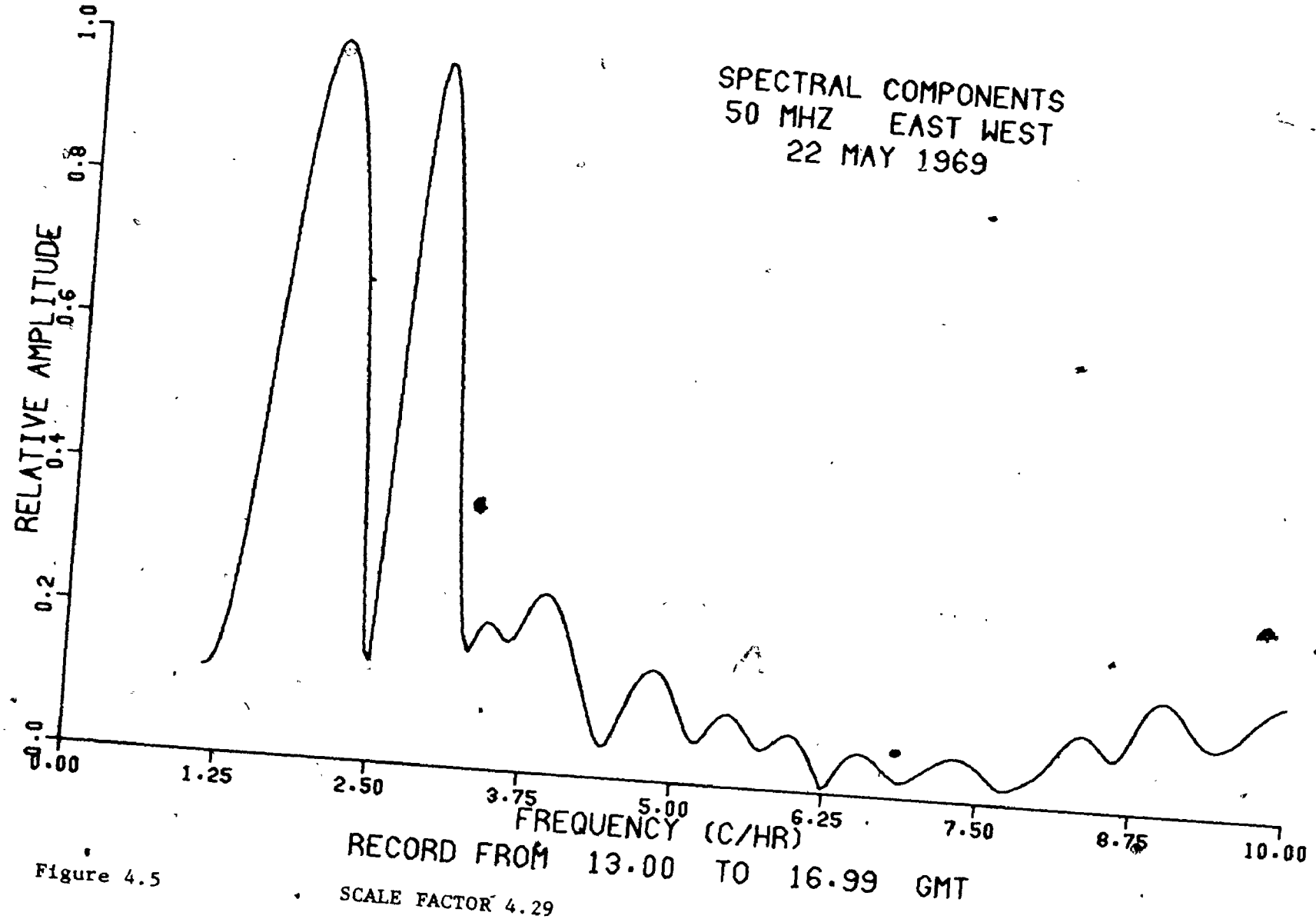

Figure 4.5

SCALE FACTOR 4.29

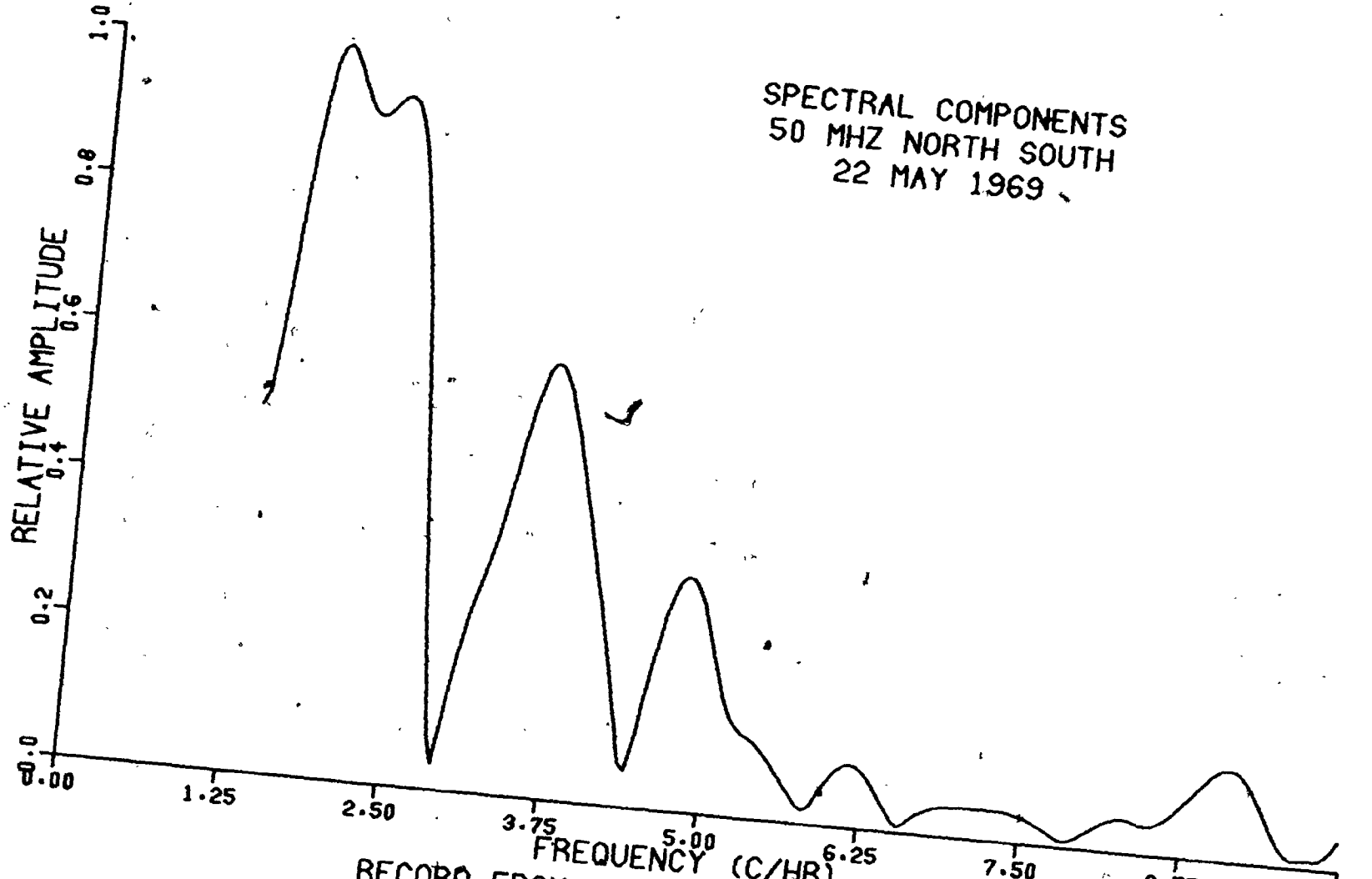

Figure 4.6

SCALE FACTOR 1.76

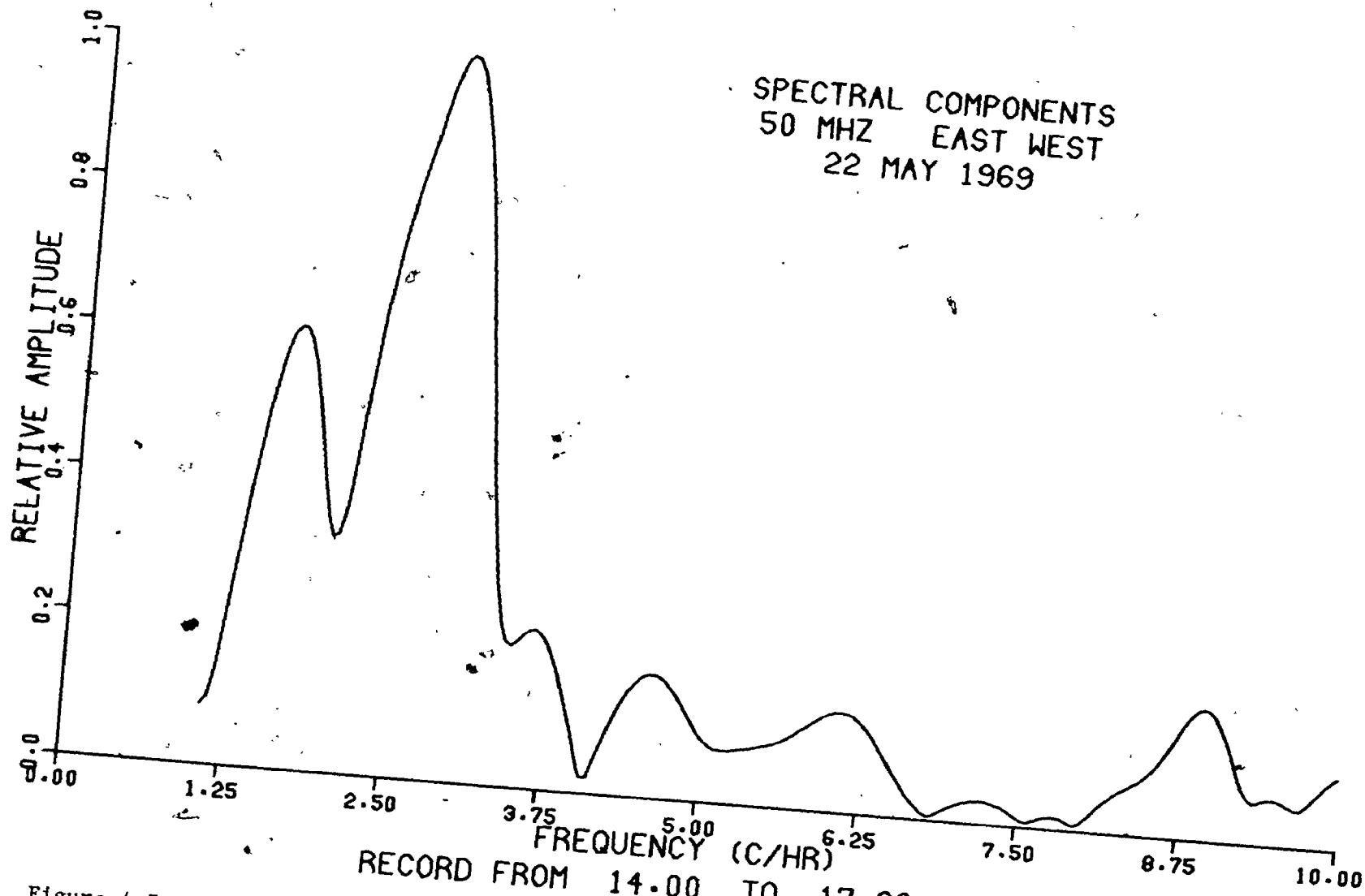
SPECTRAL COMPONENTS
50 MHZ EAST WEST
22 MAY 1969
RELATIVE AMPLITUDE
0.0
0.2
0.4
0.6
0.8
1.0
0.00
1.25
2.50
3.75
5.00
6.25
7.50
8.75
10.00
FREQUENCY (C/HR)
RECORD FROM 14.00 TO 17.99 GMT
SCALE FACTOR 2.99

Figure 4.7

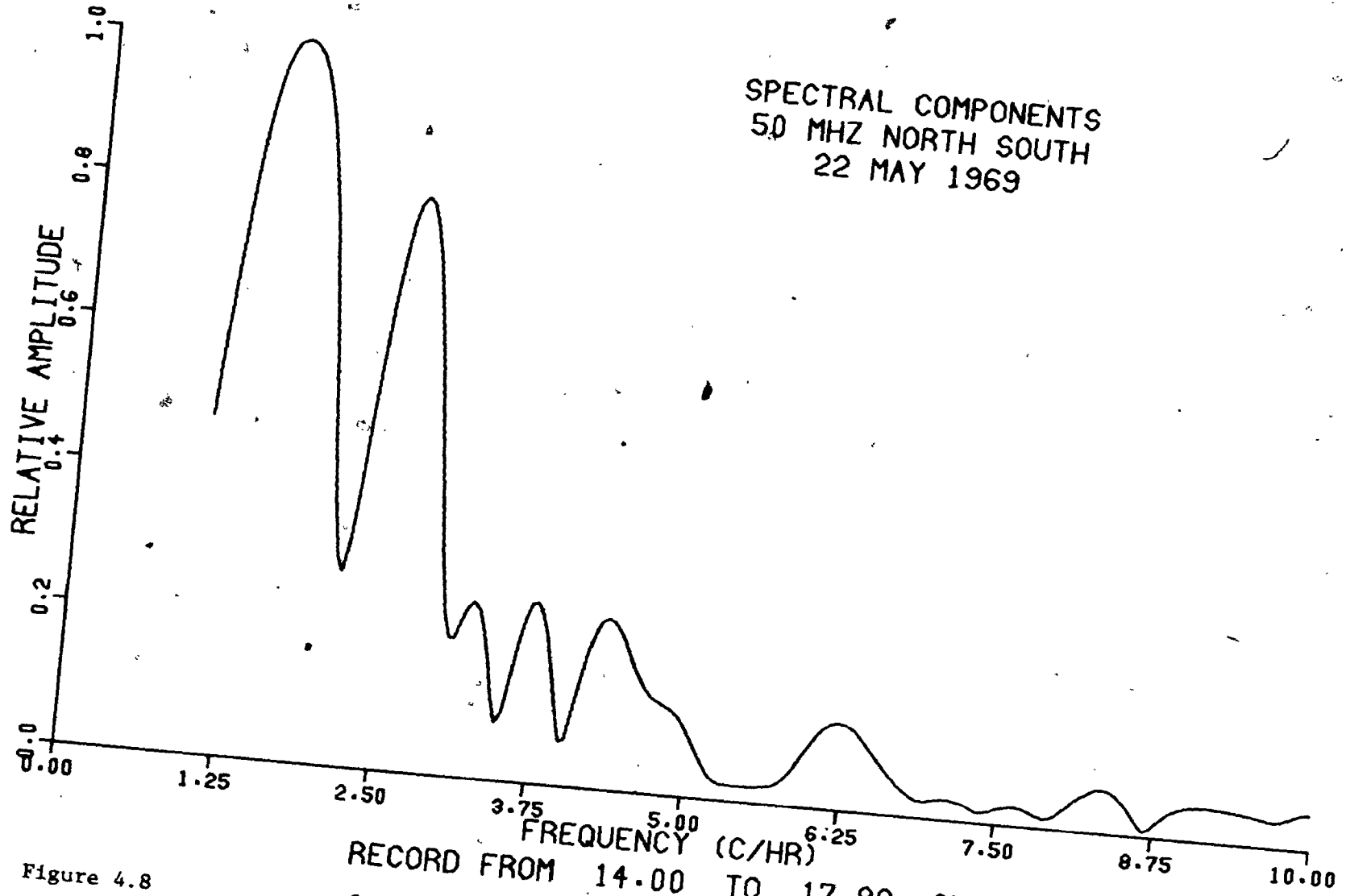

Figure 4.8

SCALE FACTOR 1.66

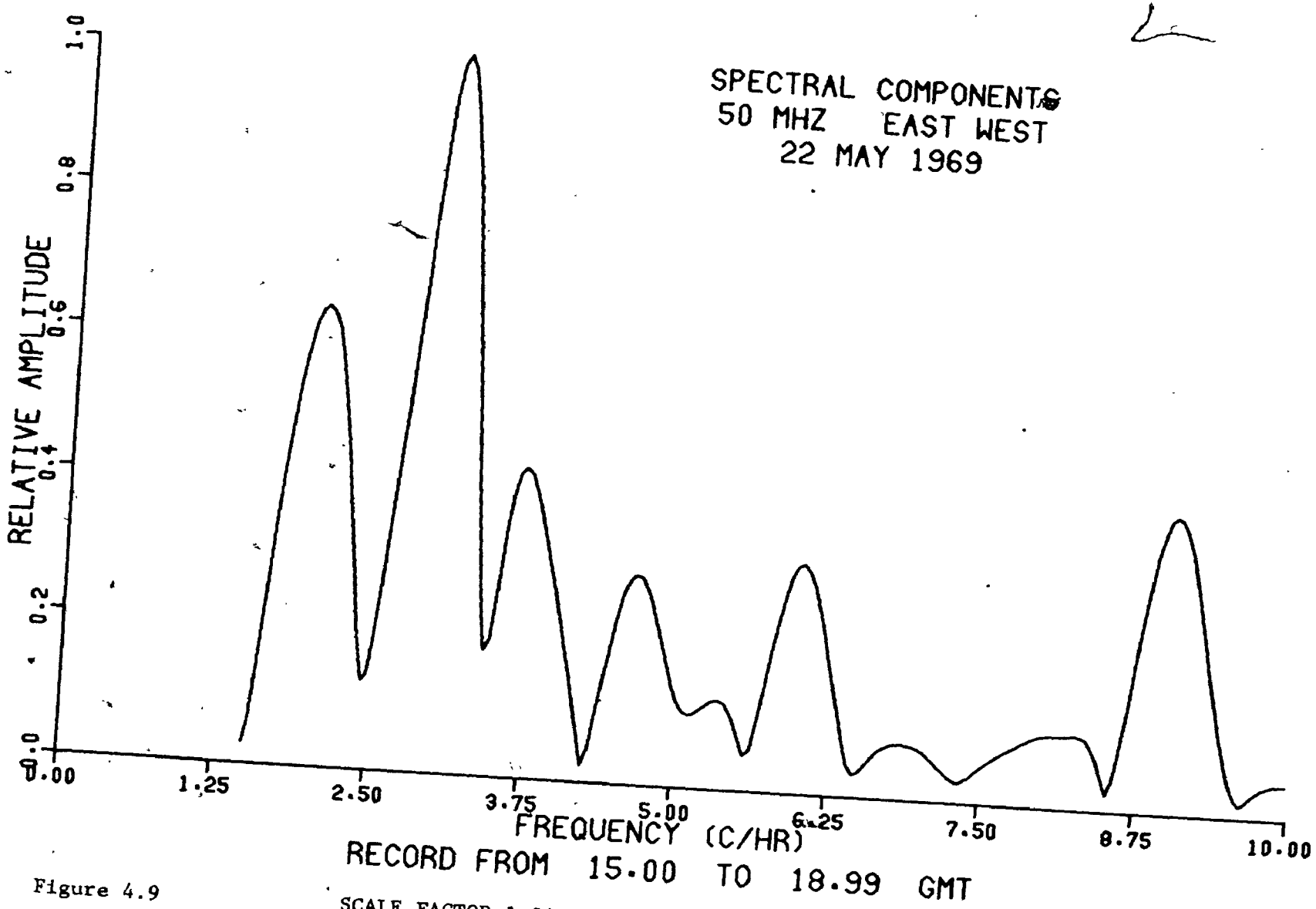

Figure 4.9

SCALE FACTOR 1.51

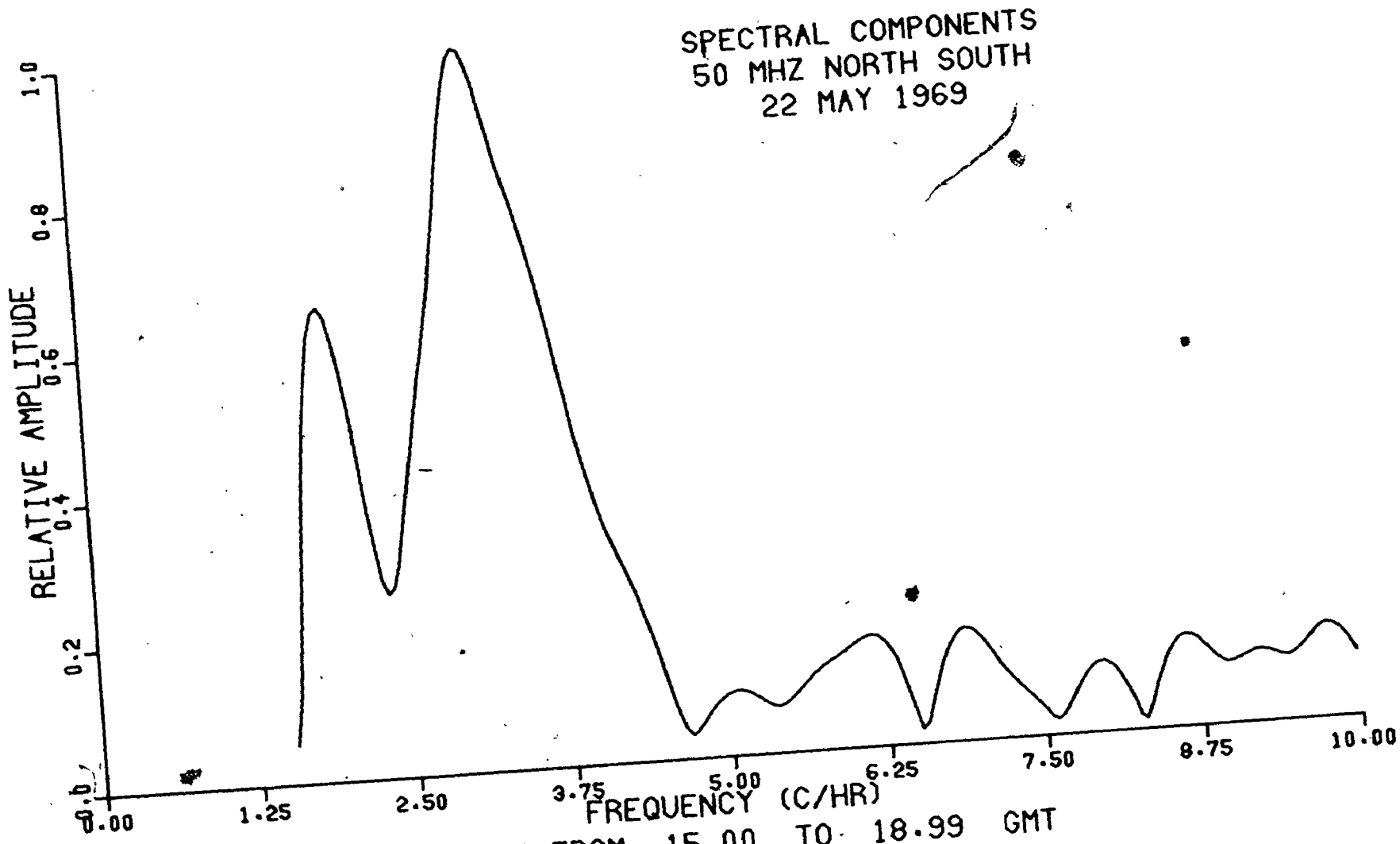

SCALE FACTOR 1.05

Figure 4.10

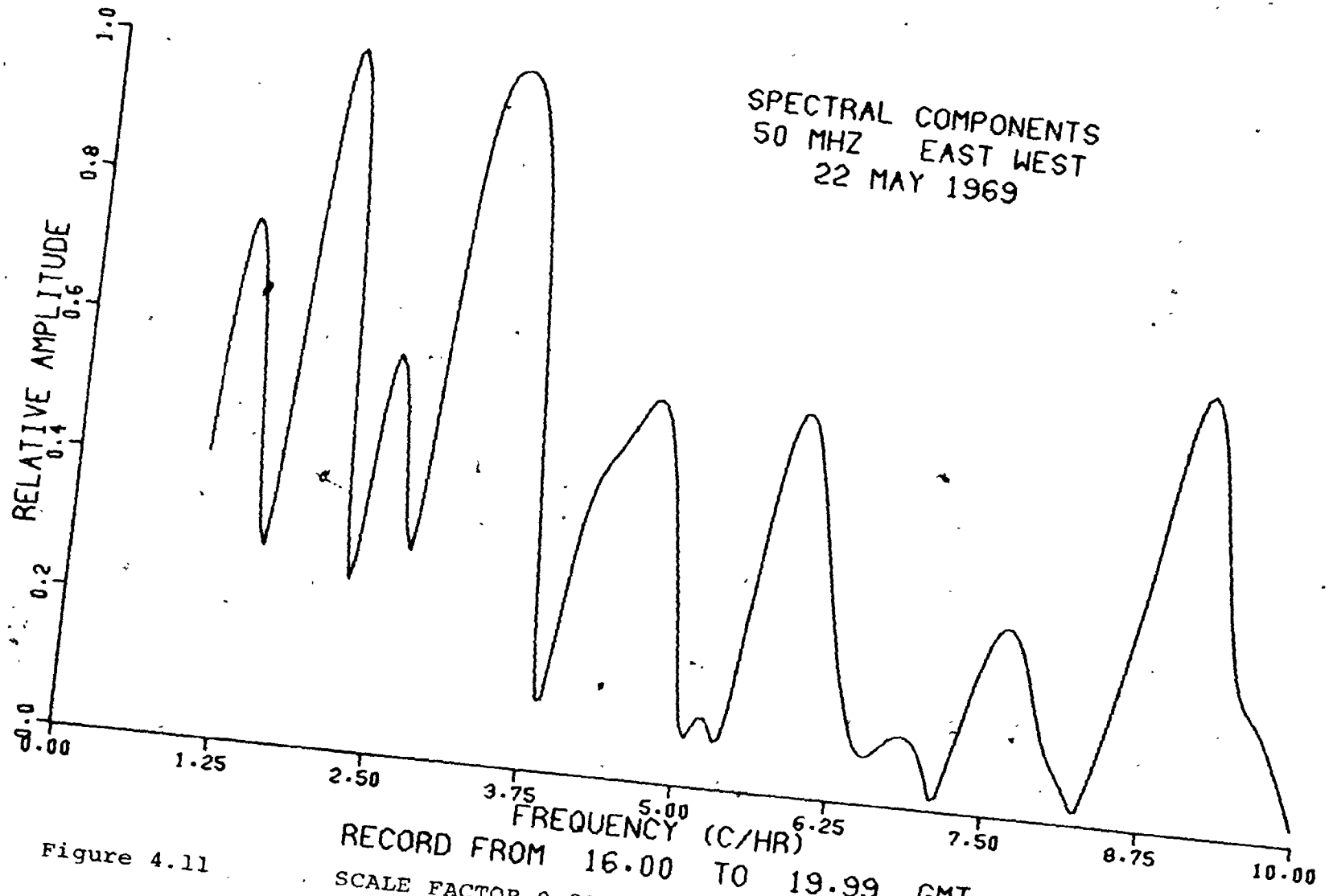
SPECTRAL COMPONENTS
50 MHZ EAST WEST
22 MAY 1969
RELATIVE AMPLITUDE
0.0
0.2
0.4
0.6
0.8
1.0
0.00
1.25
2.50
3.75
5.00
6.25
7.50
8.75
10.00
FREQUENCY (C/HR)
RECORD FROM 16.00 TO 19.99 GMT
SCALE FACTOR 0.80

Figure 4.11

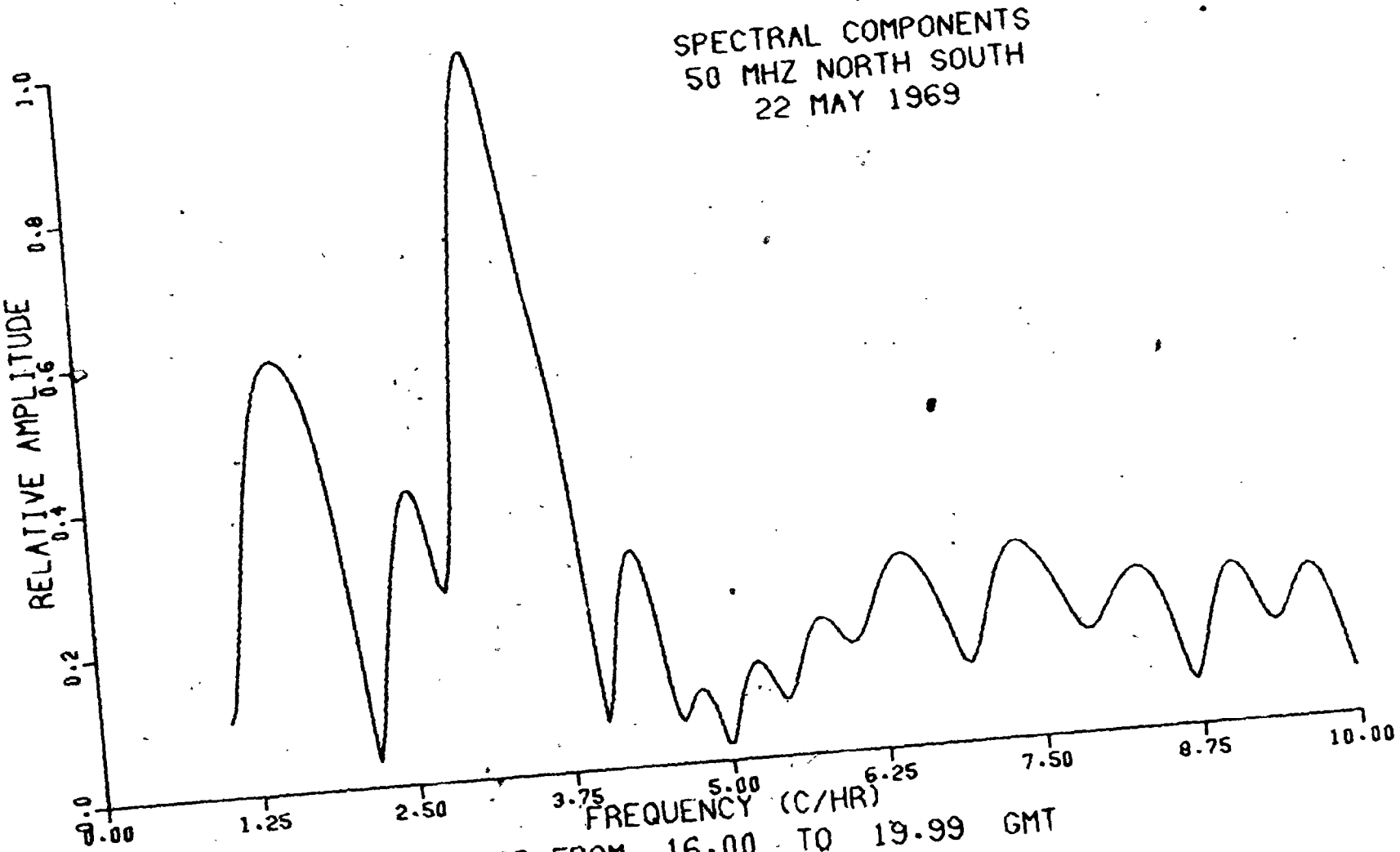
SPECTRAL COMPONENTS
50 MHZ NORTH SOUTH
22 MAY 1969
RELATIVE AMPLITUDE
0.0
0.2
0.4
0.6
0.8
1.0
0.00
1.25
2.50
3.75
5.00
6.25
7.50
8.75
10.00
FREQUENCY (C/HR)
RECORD FROM 16.00 TO 19.99 GMT
SCALE FACTOR 0.91

Figure 4.12

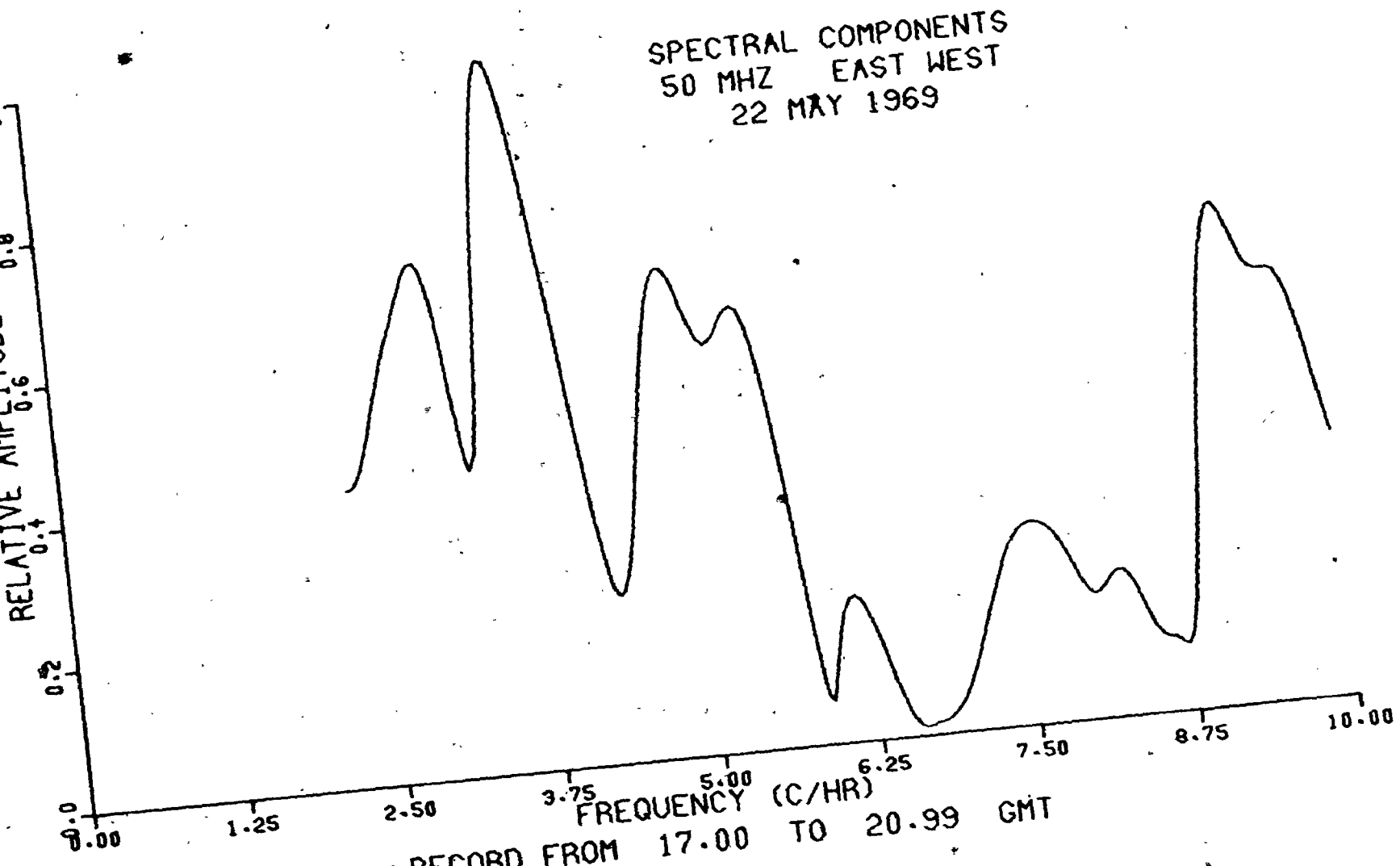
SPECTRAL COMPONENTS
50 MHZ EAST WEST
22 MAY 1969
RELATIVE AMPLITUDE
0.0
0.2
0.4
0.6
0.8
1.0
0.00
1.25
2.50
3.75
5.00
6.25
7.50
8.75
10.00
FREQUENCY (C/HR)
RECORD FROM 17.00 TO 20.99 GMT
SCALE FACTOR 1.02

Figure 4.13

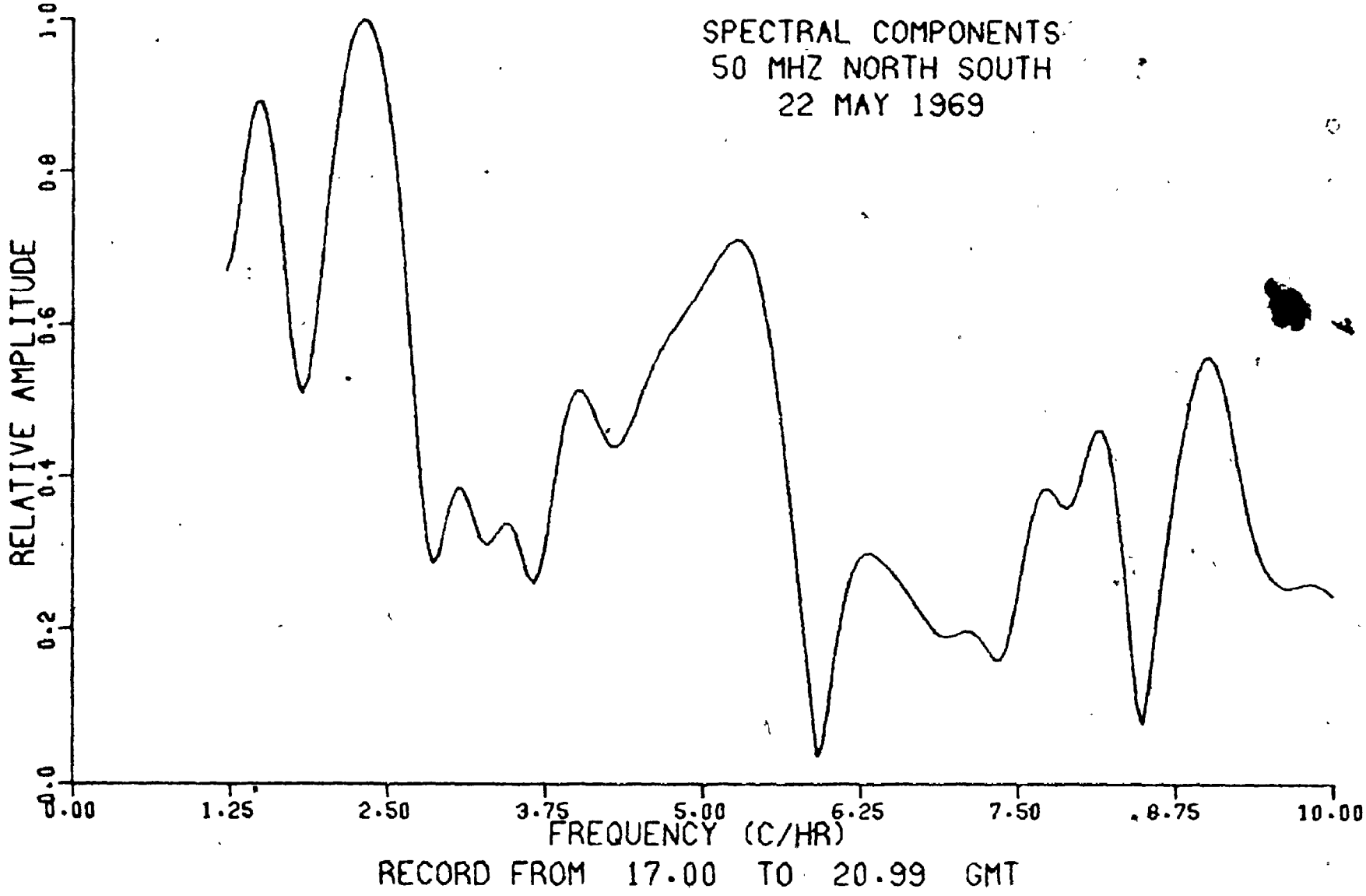

Figure 4.14 SCALE FACTOR 0.89

in the north-south record is more clearly resolved and more closely resembles the peaks in the spectrum from the other orientation.

The pair of spectra for the four hours beginning at 1500 UT closely resemble each other, at least at the low frequency end, if the broad peak of Fig. 4.10 is considered to have hints of other components, which appear to be better resolved in Fig. 4.9, representing the east-west antenna orientation. Again, the scale factors have decreased, and it is difficult to say just how much confidence can be placed in some of the spectral peaks which appear. This comment is especially true of the spectra represented in Figs. 4.11 through 4.14, where, in the north-south cases, the scale factors have dropped below one minute of arc.

In general, the spectral peaks are well-defined, although sometimes fairly broad. Similarities between the records from east-west and north-south orientations are to be expected in view of the similarity between equations 2.34 and 2.35, but small differences are also to be expected because of the $\sin(\alpha)$ or $\cos(\alpha)$ terms in those equations. Each interferometer will be sensitive to its own set of ionospheric fluctuations, whether large or small, with many disturbances showing up on both sets of data. Cross-correlation coefficients for different times of the data of Figs. 4.1 and 4.2 ranged from 0.4 to 0.7, similar to values from the simulated test data for a number of waves.

The directions of propagation of the travelling disturbances represented by the two large, low-frequency peaks present in Figs. 4.7 to 4.12 can be calculated, as indicated earlier. The decrease of amplitude throughout the day indicates an eastward component of motion,

and since the east-west variations are larger than the corresponding north-south variations, the direction of travel was more east than south. The results of the calculations are summarized in Table 4.2. (In the table, the corrected ratios are the ratios of the amplitudes adjusted for the slowly-varying normalization factors of equations 2.34 and 2.35). If the direction of the 20 minute wave is constant, it must be given with a large uncertainty (possibly 65° ± 15°.) However, it is likely that the direction of propagation is not constant, but changing throughout the course of the day. The directions calculated for the other wave are more consistent, but the period appears rather uncertain. Actually this is a consequence of the portion of the spectrum under consideration, and the uncertainty in frequency is comparable for both cases. These calculations were made on the assumption that all ionospheric and wave parameters remained constant over a period of six hours, a lot to demand of a medium such as the earth's ionosphere.

As previously stated, maximum angle of arrival variations occur when the line of sight is aligned with both the direction of wave travel and the wave front tilt. On 22 May, 1969, the solar zenith angle was 47° at 1400 UT and decreased to 22° at local noon. In view of the constant decrease in the amplitude of variations on that day, it is concluded that the angle between the line of sight and wavefront tilt was always increasing, and so the wavefront tilt of the 20-minute wave was greater than 45-50°. If conditions at the time were such that equation 2.24 was valid, and if the true wave period was around 25 minutes instead of the observed 20-22 minutes, the wavefront tilt can be estimated at 50°. This would be for a height of 250 km;

TABLE 4.2

Directions of Travel Calculated for Two Waves Identified From Data of 22 May 1969

Time of Record (UT)	Period (Minutes)	East-West Amplitude	North-South Amplitude	Corrected Ratio	Direction of Travel (E of S)
1400 - 1800	22	2.99	1.32	2.21	81°
1500 - 1900	19	1.51	1.05	1.48	70°
1600 - 2000	19	0.79	0.91	0.86	50°
1400 - 1800	38	1.82	1.66	1.07	56°
1500 - 1900	31	0.97	0.69	1.45	68°
1600 - 2000	35	0.80	0.54	1.47	70°

a vertical wavelength of 50-100 km would mean a horizontal wavelength of 75-125 km. Similar arguments for the other case of Table 4.2, assuming a period of 40 minutes, gives a wavefront tilt of 66°, and a horizontal wavelength of 110-225 km if the vertical wavelength is in the 50-100 km range.

Of potential interest on the records of Figs. 4.1 and 4.2 are the rapid (6 to 8 minute) fluctuations toward the end of the observation period. On the east-west record, because of the continuous increase in amplitude and period, they exhibit the characteristics of a short period, westward moving TID such as reported by Litva (1972). However, on the north-south record, the period is decreasing, not increasing, as theory predicts for such a travelling disturbance.

The geometry of the east-west receiving system is such that the period of the phase ramps is a minimum of just under five minutes at local noon, and increases to eight minutes by 2100 UT. The variations of Fig. 4.1 after 1930 UT follow just this increase in period. The north-south geometry is somewhat different in that the phase ramp period is decreasing at that time of day (and has a value of 7 minutes at 2000 UT) just as do the fluctuations in the record of Fig. 4.2. The original records show that the received signal was weakening late in the day, and the unfortunate conclusion is that these rapid variations come from the equipment as a consequence of the system geometry at a time of low received signal. This will, at most, obscure other variations at similar frequencies, and the periods of primary interest in this study are greater than 10-12 minutes. The sections of the two records are not without significance, however, in that the major trend late in the day exhibits a long period (greater

than two hours) variation such as those detected at this institution by means of a geostationary satellite (Webster, 1974, private communication), and for this reason, the entire records have been retained.

Data for 17 November, 1970 are shown in Figs. 4.15 and 4.16. Both sets of data are for an east-west antenna orientation, but the second graph represents variations at 150 MHz. For the time period common to both sets of data, the frequency spectra are shown in Figs. 4.17 and 4.18. Equation 2.36 suggests that similar spectra should be observed, but the $1/f_o^2$ term ensures that the variations at 150 MHz will be considerably smaller than those at 51.7 MHz. This is essentially borne out, since the dominant peak of period 15 minutes from the 150 MHz record is clearly also a dominant peak at 50 MHz, and the positions of the lower frequency peaks coincide on both records, even though the relative amplitudes don't fall perfectly into place. The actual amplitude ratio of the 15 minute period is about 5, but the ratio of the two lower frequency peaks are 8 and 12, respectively. The theoretically expected ratio is 8.4, and so the experimental values represent a wide range.

The data for this particular day represented the clearest case of similarity between the 51.7 MHz records and the 150 MHz records, and in view of the previous discussion on wavefront tilts, it is significant that the similarity was most clearly defined during wintertime observations. The solar zenith angle for that particular day was never less than 60°, and if a number of waves with wavefront tilts greater than 45-50 were present, large variations in angle of arrival can be expected. The variations in Fig. 4.15 are larger than

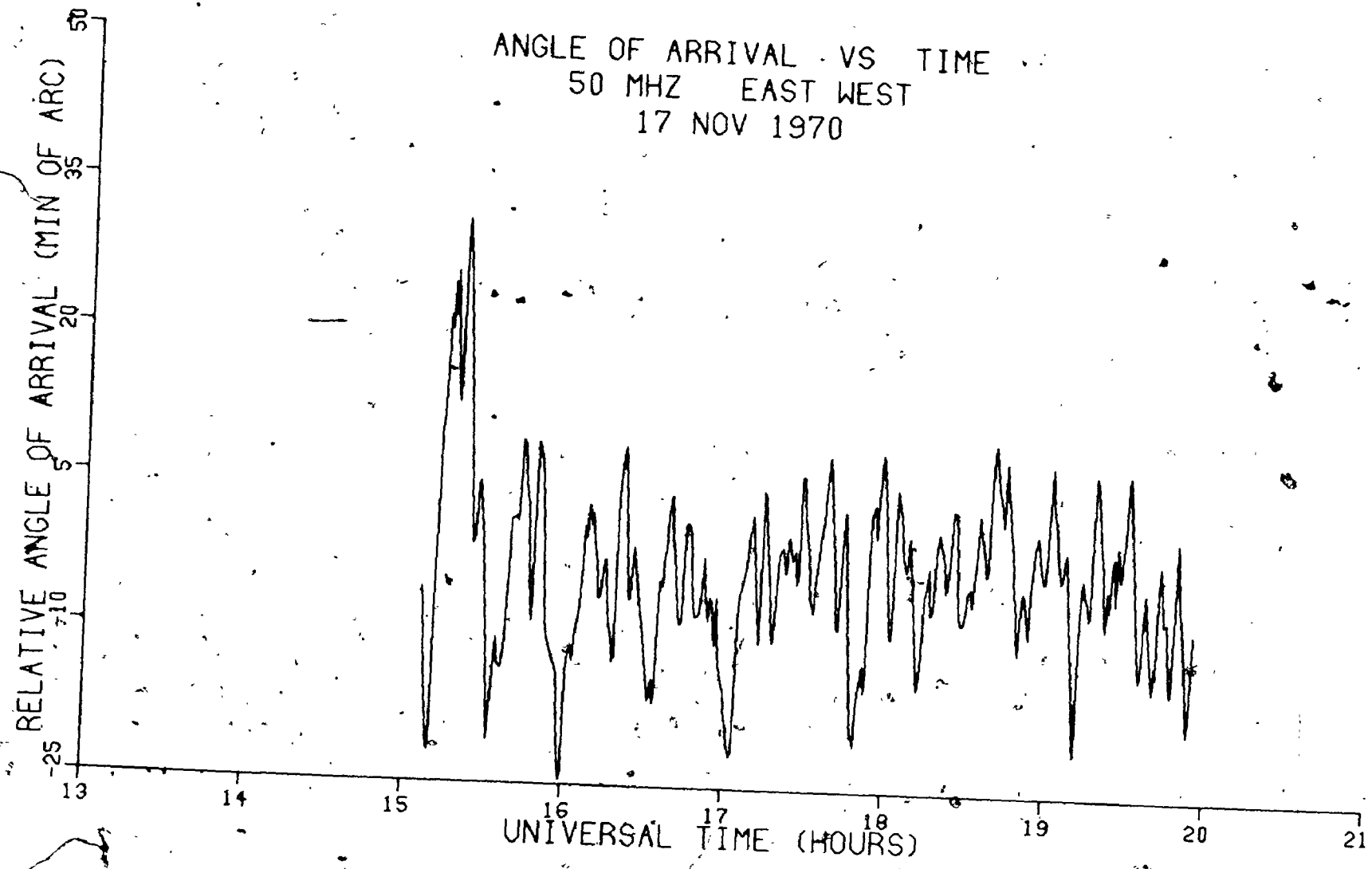
ANGLE OF ARRIVAL VS TIME
50 MHZ EAST WEST
17 NOV 1970
RELATIVE ANGLE OF ARRIVAL (MIN OF ARC)
50
35
20
5
-10
-25
13
14
15
16
17
18
19
20
21
UNIVERSAL TIME (HOURS)

Figure 4.15

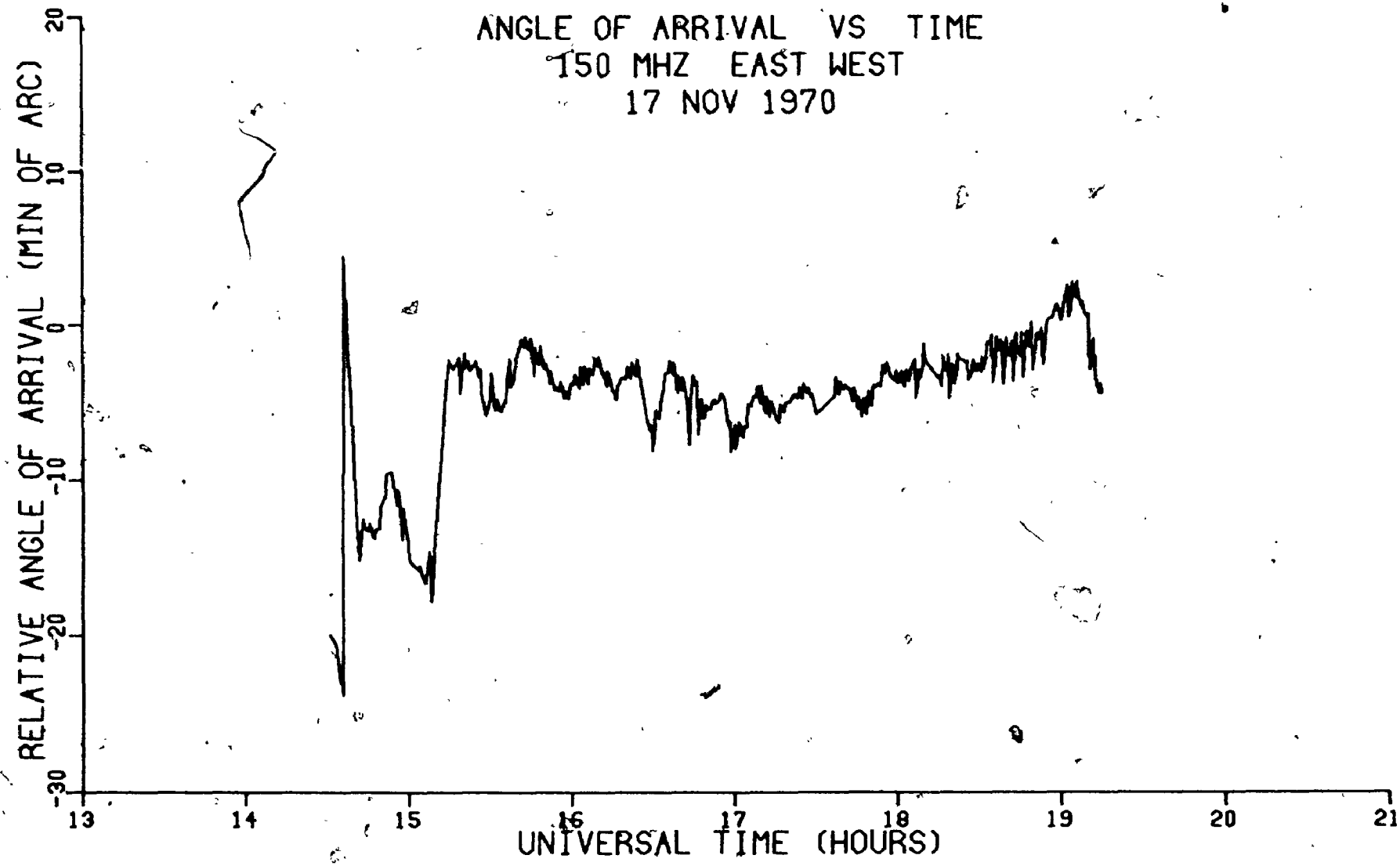
ANGLE OF ARRIVAL VS TIME
150 MHZ EAST WEST
17 NOV 1970
RELATIVE ANGLE OF ARRIVAL (MIN OF ARC)
20
10
0
-10
-20
-30
13
14
15
16
17
18
19
20
21
UNIVERSAL TIME (HOURS)

Figure 4.16

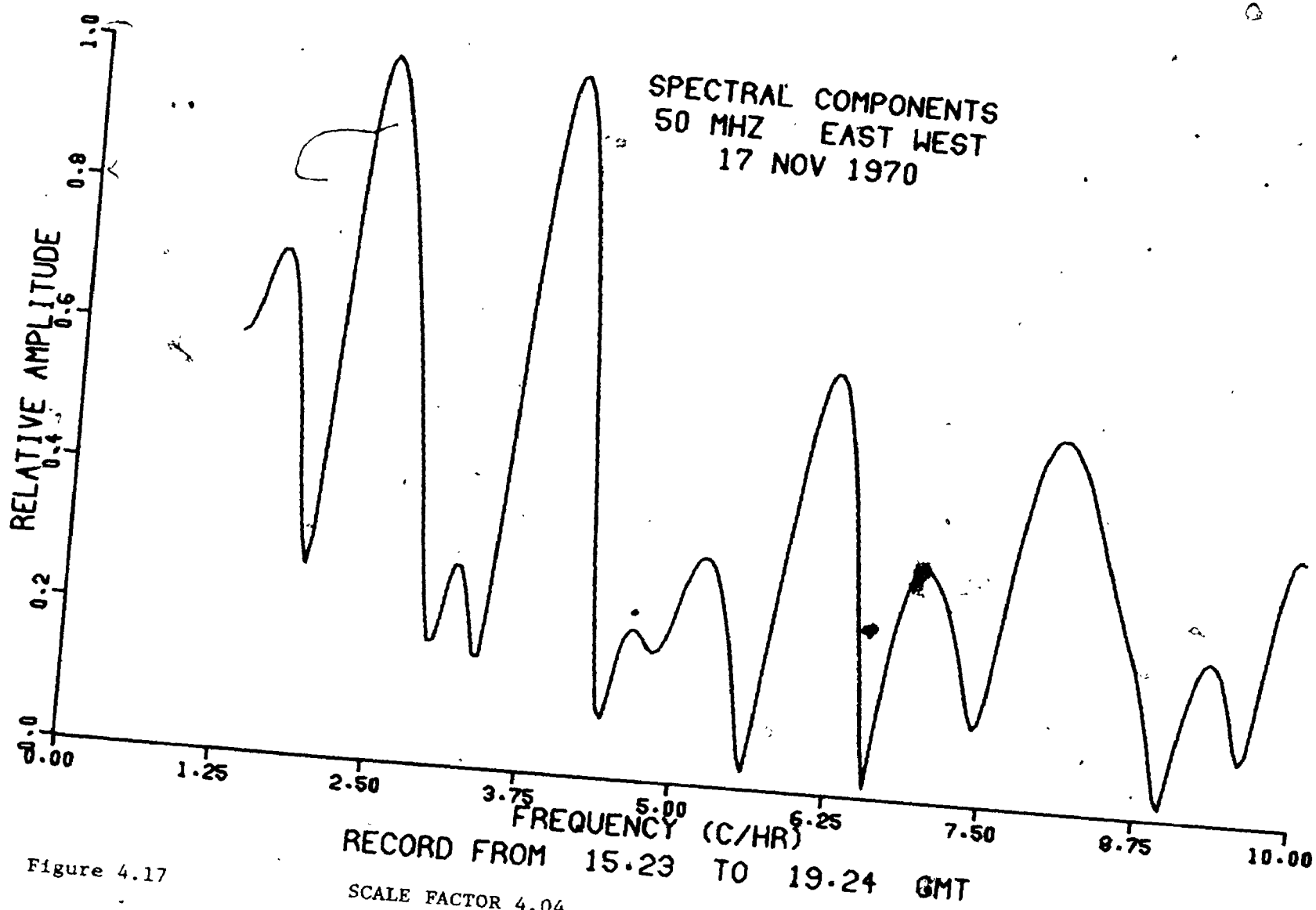

Figure 4.17

SCALE FACTOR 4.04

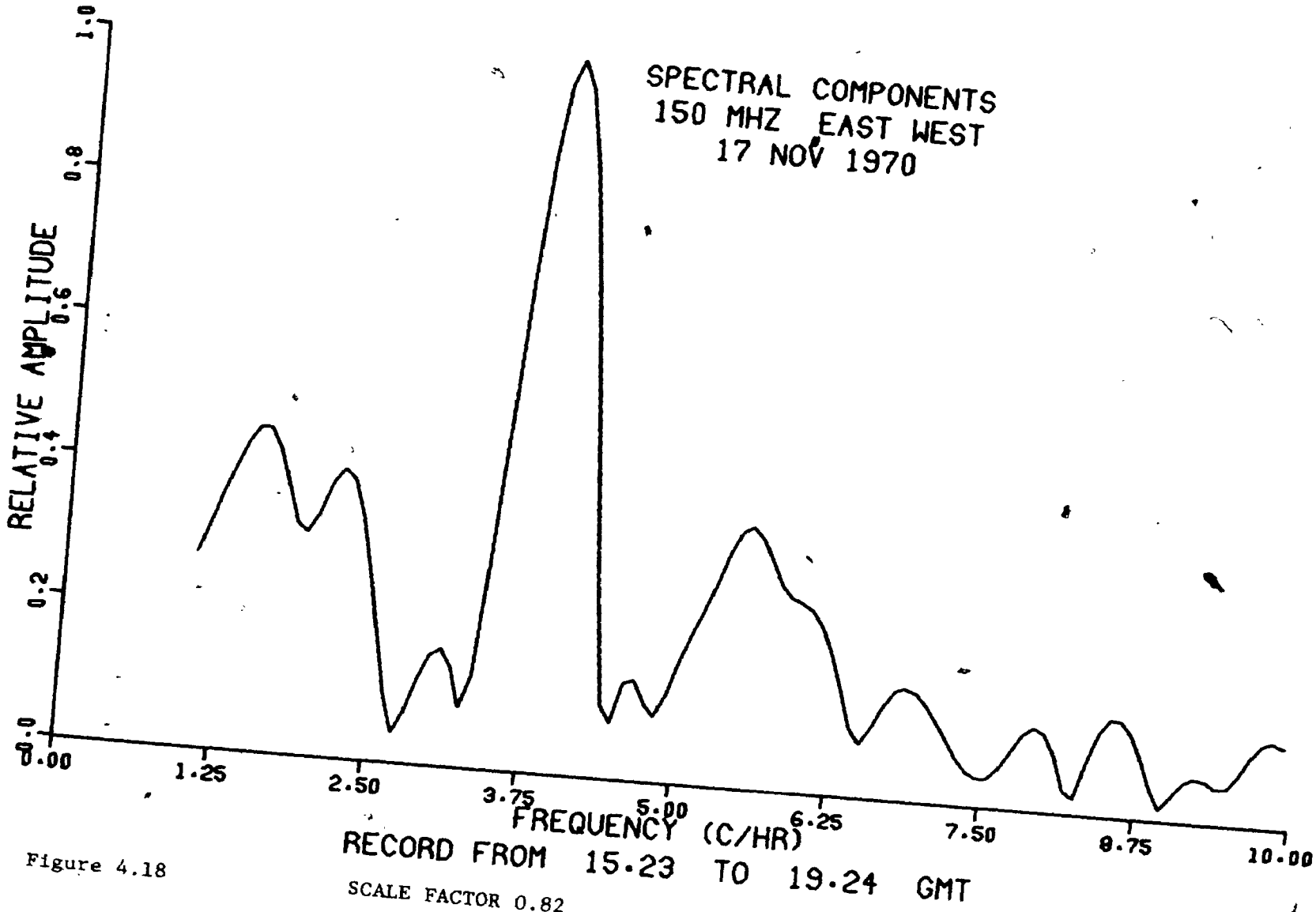
SPECTRAL COMPONENTS
150 MHZ EAST WEST
17 NOV 1970
RELATIVE AMPLITUDE
0.0
0.2
0.4
0.6
0.8
1.0
0.00
1.25
2.50
3.75
5.00
6.25
7.50
8.75
10.00
FREQUENCY (C/HR)
RECORD FROM 15.23 TO 19.24 GMT
SCALE FACTOR 0.82

Figure 4.18

those of Fig. 4.1, and it was found that this was generally true in a comparison of winter observations with summer observations.

Several hours of continuous recording were required to adequately observe the presence of ionospheric waves, and in all, data for seven different days (the latest of which was 6 January, 1973) were analysed. Since sections of the equipment at times were not operational, data for all orientations and frequencies (50 MHz east-west, 50 MHz north-south, and 150 MHz east-west) were not always available.

For the 150 MHz observations, a large percentage of the periods observed are greater than 15 minutes, an expected result, since the higher frequency radio waves are less affected by perturbations in the lower ionosphere because of the smaller values of electron density. High frequency (short period) gravity waves are damped out before reaching F region heights. E region effects, however, appear on the 50 MHz records, as evidenced by the large number of periods across the whole spectrum. Variations are observed to be greater during the winter than during the summer, chiefly because the elevation of the line of sight is such that it tends to align more closely with the wave fronts of ionospheric wave disturbances when the sun's declination is negative. Observations at 150 MHz indicate that disturbances can be detected at this frequency, but the amplitude of variations is very small compared with the observations at a lower frequency. Some results using satellite beacons at 150 MHz will be discussed.

4.3 Satellite Measurements

It was hoped to be able to use angle of arrival data obtained from the 150 MHz beacons on the Transit series of satellites to determine the spatial size, or horizontal wavelength, of gravity wave induced travelling ionospheric disturbances observed with the solar interferometer. Titheridge (1963) gives a simple equation to estimate the size of large-scale irregularities given the satellite velocity, height, disturbance height, and the temporal variation. Unfortunately, whenever the sun was active, the satellites were either in an unfavorable position in the sky, or passing by at the wrong time of day to be of any use in conjunction with the data from the sun.

However, expected variations can be calculated using equation 2.34 and satellite position information. The satellite parameters used were those for Satellite 30130/40 which crossed the equator going north at 1428 UT on 10 May, 1971, at a west longitude of 69.4° (cf receiving site longitude of 81.3°). Even though the satellite's longitude increases westward with increasing latitude, the look azimuth for this pass moved from almost south towards the east as the satellite moved northward. The reason for this is that the change in longitude is very slow compared with the change in latitude. To calculate the theoretical variation in the angle of arrival due to a gravity-wave induced TID, the satellite height was assumed constant at 1100 km. The following ionospheric and wave parameters were adopted for the calculations:

$h = 50$ km $\qquad\qquad$ $a = 0.1$

f_o = 150 MHz N_o = 5 x 10^{11} m^{-3}

λ_x = 175 km λ_z = 100 km

z_o = 300 km Period = 30 minutes

Three values of azimuth: 30° E of S,

30° W of S,

and due east.

The results of the calculations are shown in Figs. 4.19, 4.20, and 4.21. A similar calculation was made with a wave azimuth of -90° (due west), but the variations were at least two orders of magnitude smaller than the ones presented, and so such a wave would go entirely undetected using that particular satellite passage.

It is clear that the number of wave periods observed is very dependent on the azimuth of propagation. Since it also depends on the horizontal wavelength, the absolute determination of λ_x is extremely difficult. The fact that the period of variation is continuously changing can be understood intuitively, since the higher the zenith angle, the longer time it will take the ray path to traverse a complete wavelength. The effect of focussing can be seen by the changing amplitude of the variations.

The experimental results from the satellite pass just described are given in Fig. 4.22. The angle of arrival curve for the entire pass appears very smooth on a large scale, and Fig. 4.22 represents the variations observed after the removal of the trend over the entire pass. The large scale variations are attributed to a gravity-wave induced TID because the time scale of 60 to 70 seconds and amplitude variations of two to three minutes of arc are consistent with the theory presented here. Small variations of the order of

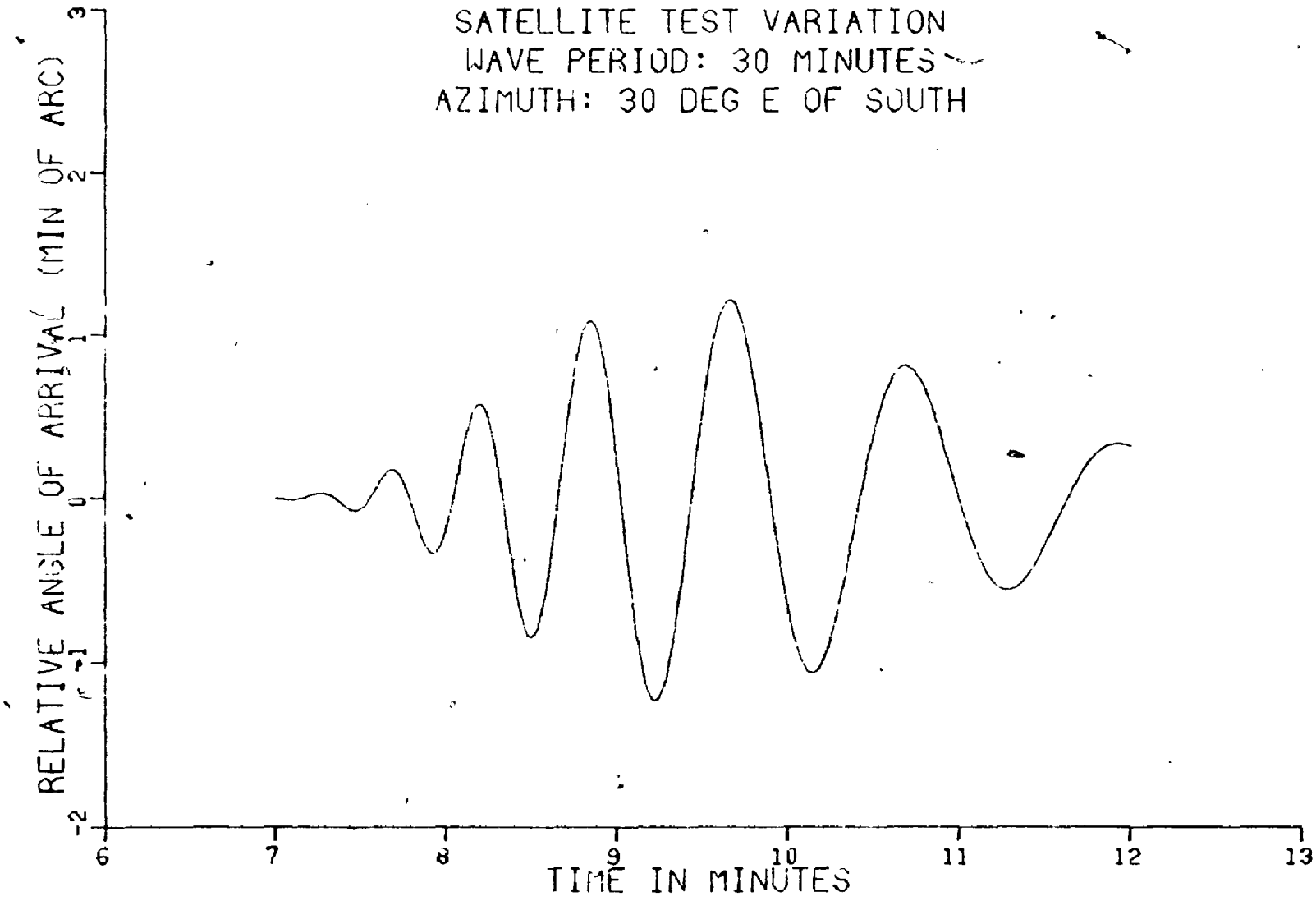
SATELLITE TEST VARIATION
WAVE PERIOD: 30 MINUTES
AZIMUTH: 30 DEG E OF SOUTH
RELATIVE ANGLE OF ARRIVAL (MIN OF ARC)
3
2
1
0
-1
-2
6
7
8
9
10
11
12
13
TIME IN MINUTES

Figure 4.19

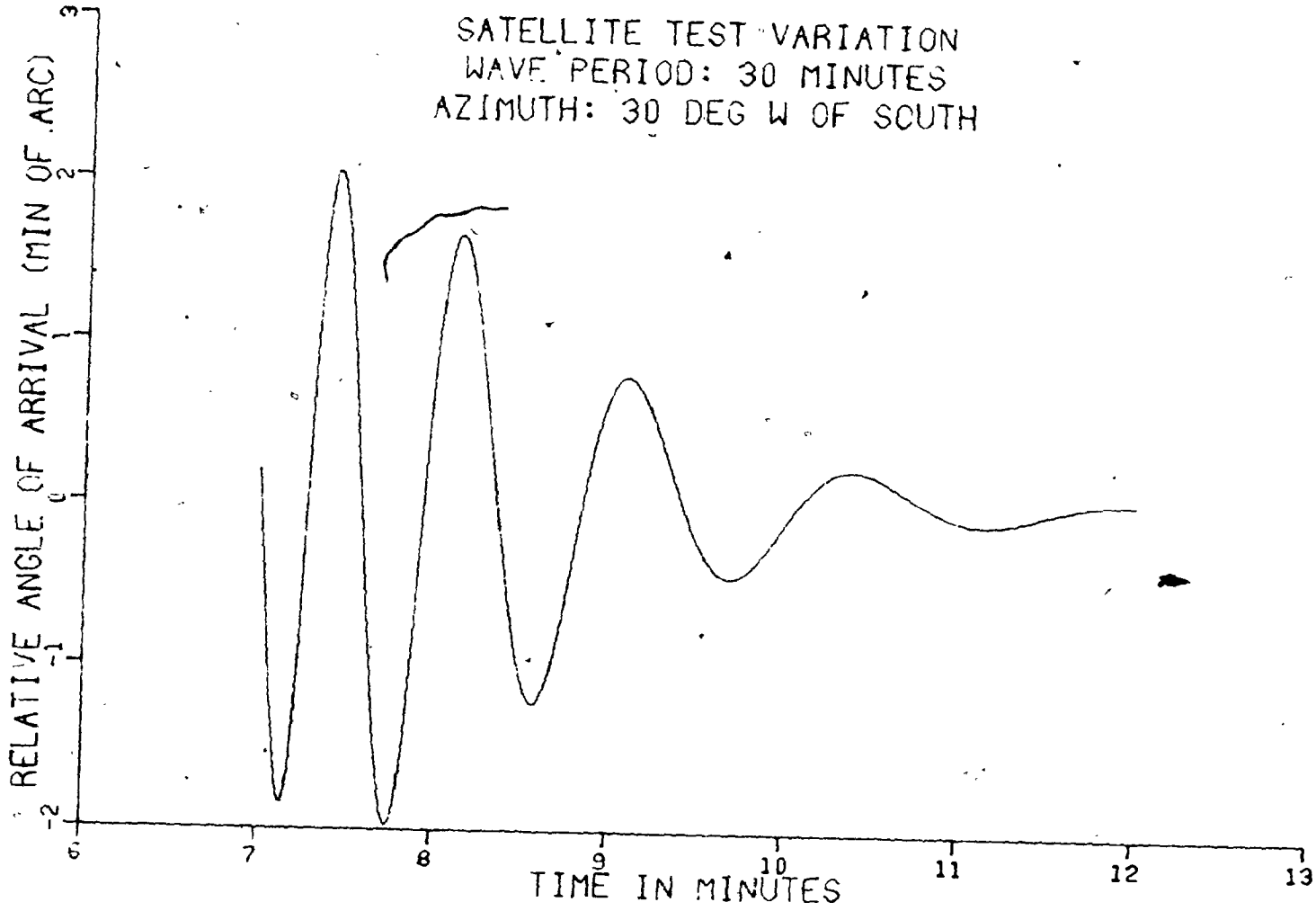
SATELLITE TEST VARIATION
WAVE PERIOD: 30 MINUTES
AZIMUTH: 30 DEG W OF SOUTH
RELATIVE ANGLE OF ARRIVAL (MIN OF ARC)
3
2
1
0
-1
-2
6
7
8
9
10
11
12
13
TIME IN MINUTES

Figure 4.20

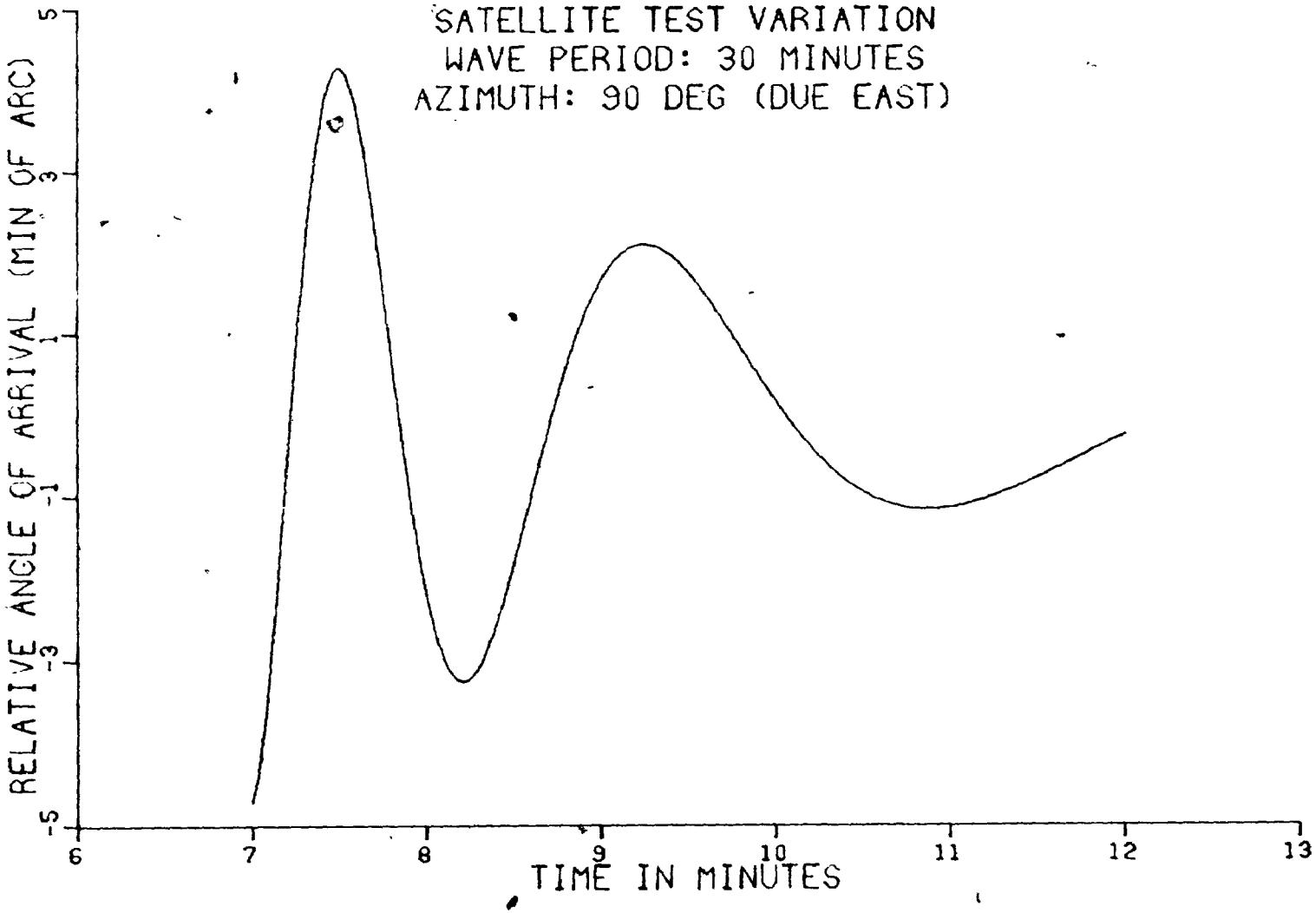
SATELLITE TEST VARIATION
WAVE PERIOD: 30 MINUTES
AZIMUTH: 90 DEG (DUE EAST)
RELATIVE ANGLE OF ARRIVAL (MIN OF ARC)
5
3
1
-1
-3
-5
6
7
8
9
10
11
12
13
TIME IN MINUTES

Figure 4.21

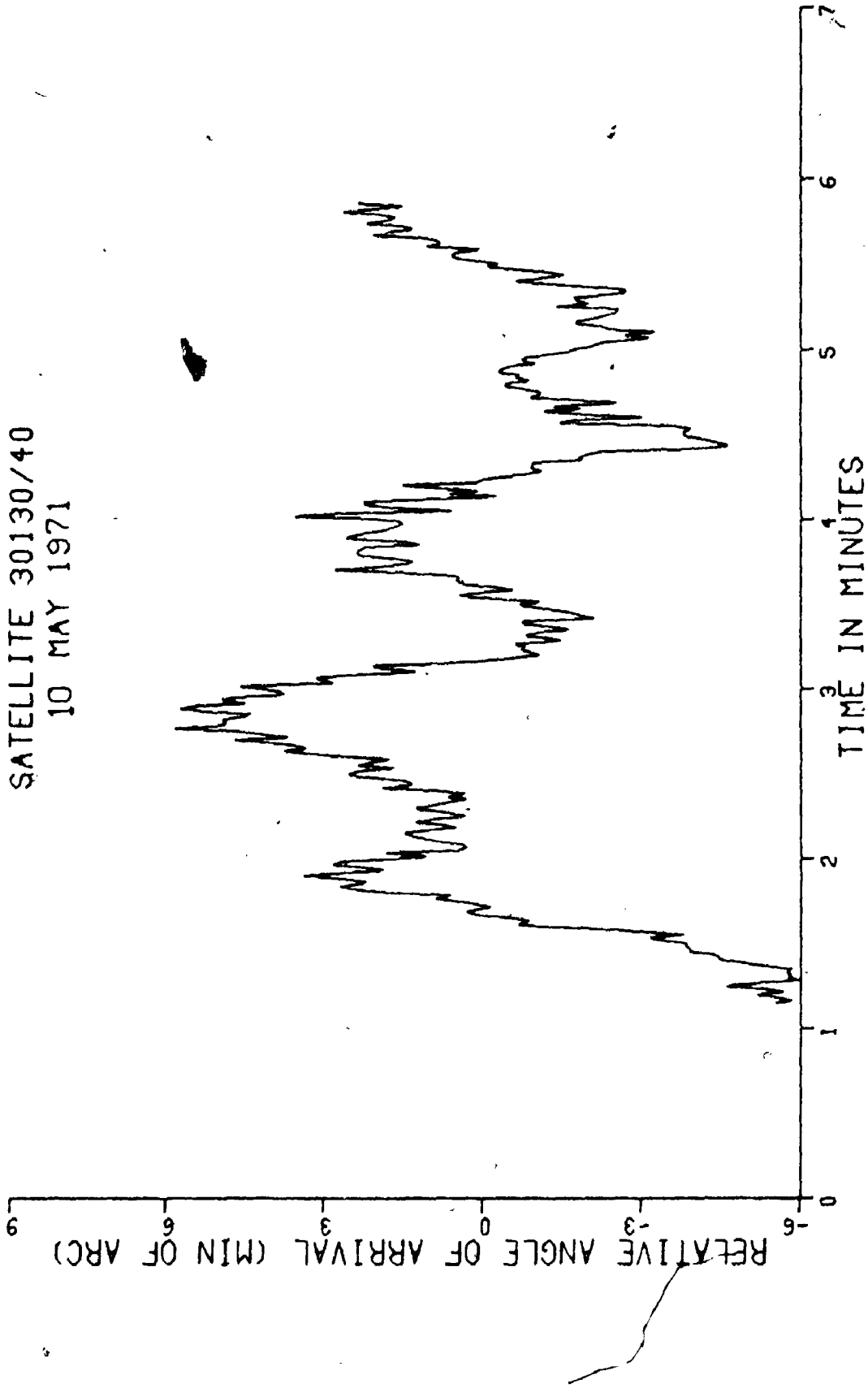
SATELLITE 30130/40
10 MAY 1971
RELATIVE ANGLE OF ARRIVAL (MIN OF ARC)
9
6
3
0
-3
-6
0
1
2
3
4
5
6
7
TIME IN MINUTES

Figure 4.22

four or five seconds are also present, but these must be due to irregularities of spatial size considerably smaller than the values of TID wavelengths generally reported in the literature.

4.4 Difficulties in Using the Sun as a Source to Study Ionospheric Gravity-Waves

The results of the spectral analysis of the angle of arrival variations of solar metric radio waves give an indication of the difficulties involved in determining the parameters of the gravity-wave induced travelling disturbances (the horizontal and vertical wavelength, the period, speed, height, and direction of propagation). The apparent period is determined from the spectral analysis, and the direction of travel can be calculated from the relative amplitudes from the baselines of ~~two orientations~~. All other wave parameters must be estimated making certain assumptions about the ionosphere and the theoretical behaviour of the waves.

The behaviour of the amplitude of variations leads to an estimate of the wavefront tilt, and when the direction of wave travel has been calculated, the actual wave period can be estimated. The wavefront tilt and period yield a value for t_g, the gravity-wave cutoff period, and this gives an approximate value for the height of the disturbance. Also, the wavefront tilt gives the ratio of horizontal to vertical wavelength, and so these values can be placed within certain limits.

The wavefront tilt plays an important role in determining whether or not a particular gravity-wave induced TID is observed. If the radio ray path is normal, or almost normal to the phase fronts,

no variations will be detected because the compressions and rarefactions of the electron density perturbation will effectively cancel each other out, and it is the total effect along the ray path which is detected. If, on the other hand, the ray path is almost parallel to the phase fronts, the integrated effect will be large, and the effect of focussing will be evident. For this reason no south to north travelling disturbances are observed.

The period observed can be significantly different from the true wave period, as shown in section 4.2. A 21-minute wave, depending on its direction of travel, can be observed to have a period as low as 15 minutes or as high as 27 minutes. The observed frequency, as well as the amplitude of variation, is not constant, but changes continuously as the azimuth and elevation of the radio ray path vary throughout the day. A factor which has not been included in the calculations, but which deserves mention, is the possible effect of neutral winds in the F-region. If a component of such a wind were parallel or anti-parallel to the direction of wave travel, the observed period of the wave could be significantly altered. Values of mid-latitude F-region winds have been calculated at 100-200 m/sec (Geisler, 1966, 1967), comparable to TID speeds reported in the literature, and so periods can be changed by factors of two or more.

Ideally, of course, a given wave will leave a characteristic signature on an interferometer record. Problems in interpretation, however, do arise. The theoretical curves given earlier in this chapter were calculated assuming certain values for various ionospheric and wave parameters. These are assumed to remain constant over periods of several hours and over horizontal distances of

thousands of kilometers. If a wave were dying out, either in time or because the ray path were leaving the affected region of the ionosphere, the amplitude of the variations as determined by the spectral analysis technique would rapidly decrease in successive records since it is the effect over the entire length of record which is measured. Because of the large number of periodic and non-periodic variations present, it is generally not possible to tell from the original record just when the contribution of a given wave starts or stops. The interference of waves of slightly differing phases or frequencies can compound the difficulties in identifying given components. This problem is not unique to this method of analysis, as Hines and Rao, 1968, caution experimenters in their interpretation of three-station drift measurements for reasons just such as this.

CHAPTER 5

DISCUSSION AND CONCLUSIONS

In spite of the interpretational difficulties described in Chapter 4, the results of this study show clearly that many of the large scale variations in the angle of arrival of solar metric radio waves are due to refractions occurring in the earth's own ionosphere and that estimates of atmospheric wave parameters can be made. Solar radio wave measurements were made at 51.7 MHz with two antenna baseline orientations, and both solar and satellite beacon measurements were made at 150 MHz with a single antenna baseline.

A detailed spectral analysis was made in order to identify the dominant periods occurring in the angle of arrival data. Initially, this showed that there were many more periods present than might be expected on visual examination, and that these periods were comparable to those due to travelling disturbances in the ionosphere. The amplitudes of corresponding spectral peaks from the records of two baseline orientations permit the identification of the direction of ionospheric wave propagation. When this has been established, the true period of the wave (generally different from the observed period) can be estimated. The behaviour of the amplitudes (increase or decrease) with changing elevation of the line of sight provides information about the wavefront tilt. When this has been estimated, a range of values for the horizontal and vertical wavelength can be established

as well as approximate values for the gravity-wave cutoff period and the height of the disturbance. The actual size of angular variations indicates electron density perturbations of a few percent.

The normalized spectra of the 150 MHz solar data were found to be similar to the 50 MHz spectra of the same baseline orientation and same time of day. The variations at the lower frequency, however, were of much greater amplitude because of the frequency dependence. Direction of arrival measurements from beacon satellites show that angular variations of the order of a few minutes of arc (similar in magnitude to the solar data for the same frequency), and attributed to TID's, can be observed at 150 MHz. It is unfortunate that no satellite records are available for days when the sun was active, because these would yield information about the spatial size of irregularities.

It seems likely that in view of the wide frequency range of periodic variations which have been observed that E-region effects are present as well as those in the F-region. The records at 51.7 MHz do show a somewhat greater percentage of waves with periods greater than 12-15 minutes, but a large number are observed with periods considerably shorter. Of the variations detected at 150 MHz, about 75% have periods greater than 12-15 minutes. Because of the higher frequency, the amplitude of variations is smaller, and so in general the perturbations in the large F-region electron density will be preferentially observed. Hence the difference observed between the records at the two frequencies is not surprising.

Georges (1968) suggested four classes of TID's rather than just three which were given in Chapter 1. The fourth classification consists of a large number of incoherent, superposed gravity waves propagating to ionospheric heights from below, in which case each wave would have a maximum effect at a given height. This helps to explain the large number of waves observed over periods of several hours. MacDougall (1972) and Reddi and Rao (1971) also observed periods over a wide range, including short ones of under 10 minutes, such as were found in this study.

There is an item that is worth mentioning briefly. Ionospheric disturbances have been associated with thunderstorms (Davies and Jones, 1971), and there is a band of acoustic waves with about a 3 minute period which can propagate to ionospheric heights (Georges, 1968). One spectral analysis record at 150 MHz showed a peak at a value of 3 minutes, a period not expected of E or F region gravity waves. This was an afternoon record, and there was thunderstorm activity a few hundred kilometers to the southwest of this receiving station, so the possibility exists that an acoustic wave manifested itself as an observable ionospheric disturbance. Curry (1973), at this institution, studied gravity waves caused by thunderstorms, but unfortunately none of the tropospheric events he examined occurred at time of ionospheric investigation by the solar interferometers.

The possible effect of neutral winds on TID's was mentioned briefly in Chapter 4. If there were a large component of wind in the direction of wave travel, the observed period of the wave would be

Georges (1968) suggested four classes of TID's rather than just three which were given in Chapter 1. The fourth classification consists of a large number of incoherent, superposed gravity waves propagating to ionospheric heights from below, in which case each wave would have a maximum effect at a given height. This helps to explain the large number of waves observed over periods of several hours. MacDougall (1972) and Reddi and Rao (1971) also observed periods over a wide range, including short ones of under 10 minutes, such as were found in this study.

There is an item that is worth mentioning briefly. Ionospheric disturbances have been associated with thunderstorms (Davies and Jones, 1971), and there is a band of acoustic waves with about a 3 minute period which can propagate to ionospheric heights (Georges, 1968). One spectral analysis record at 150 MHz showed a peak at a value of 3 minutes, a period not expected of E or F region gravity waves. This was an afternoon record, and there was thunderstorm activity a few hundred kilometers to the southwest of this receiving station, so the possibility exists that an acoustic wave manifested itself as an observable ionospheric disturbance. Curry (1973), at this institution, studied gravity waves caused by thunderstorms, but unfortunately none of the tropospheric events he examined occurred at time of ionospheric investigation by the solar interferometers.

The possible effect of neutral winds on TID's was mentioned briefly in Chapter 4. If there were a large component of wind in the direction of wave travel, the observed period of the wave would be

shorter than the true period. If the wind were opposite to the direction of wave propagation, the observed period would be longer, and possibly, the appearance of standing waves might be produced. Wind components other than those parallel or anti-parallel to the direction of wave travel might cause a change in this direction. Possible evidence of this can be seen in the changing azimuth of propagation of the 20-minute wave described in Chapter 4. (Successive directions change through a total of 30°.) According to the model developed by Geisler (1966, 1967), there is a southwesterly wind component early in the day, which might account for the change in wave propagation direction. However, such a change is not observed for the other wave of the same day, so further studies should indicate either true changes in wave propagation or large uncertainties in the method of their determination.

A given TID should leave a characteristic trace on an angle of arrival record, and the calculation of a large number of characteristic curves for interferometer observations of ionospheric waves would aid in the identification of their properties. For the solar readings this would have to be done for several different values of the sun's declination in view of the different sensitivities to different wave front tilts. Parameters such as horizontal and vertical wavelength, wave period, azimuth of propagation, and electron density would also have to be varied to obtain a good representative sampling of the possibilities. This could also be done for the satellite observations, but the traces left on angle of arrival

records vary considerably for different satellite pass parameters. Hence the need for large allotments of computing time and money.

Some difficulties in using the sun as a radio beacon were outlined in Chapter 4. The method is restricted in the sense that radiation is not always emitted at a sufficiently high level, especially at times of minimum solar activity. However, when the sun is active, a wide range of frequencies for ionospheric probing can be utilized, from a few MHz to several hundred MHz, and at the present time low frequency satellite beacons are rare. Always looking generally toward the south is a point in favour of the method, since a great many TID's are observed to travel roughly in that direction, and the forward tilts of the wave fronts aid in their detection. A wide range of the sky is covered, even though specific areas are observed only at certain times of the day. Much more data could be obtained at a time of peak solar activity, and the beacons on geostationary satellites could be employed to provide night time readings and to aid in resolving ambiguities which might arise from other methods. Statistical studies of directions of travel (and changes in these values) would be useful in the identification of sources of TID's. Ideally, a "watchdog" type of data acquisition system could be employed, but it is highly unlikely that the return would justify the cost of such a system.

To conclude briefly, this study has shown how gravity wave induced travelling ionospheric disturbances can cause large variations in the angle of arrival of solar radio waves. Techniques of

spectral analysis and the fact that the sun moves relatively rapidly across the sky aid significantly in the identification of ionospheric wave parameters.

APPENDIX A

ERROR ANALYSIS IN THE MEASUREMENT OF ANGLE OF ARRIVAL

The relative angle of arrival δ is defined as

$$\delta = \theta_S - \theta_N \tag{2.3}$$

where θ_S is the angular position of the centre of the sun and is given by:

$$\cos\theta_S = \sin(HA)\cos(D) \tag{2.2}$$

and HA and D are the hour angle and declination respectively. θ_N is the angle of arrival of the noise source relative to the antenna baseline and is given by

$$\cos\theta_N = \frac{\lambda}{d}(n + \phi) \tag{2.1}$$

where ϕ is the relative phase (here, a number between 0 and 1) and n is an integer such that $-\frac{d}{\lambda} \leq n \leq \frac{d}{\lambda}$.

HA and D are given by

$$HA = UT - \left(E_o + \frac{\Delta E_o}{3600} \times \frac{UT}{24}\right) \times 15 - Long \tag{A1}$$

$$D = D_o + \frac{\Delta D_o}{3600} \times \frac{UT}{24} \tag{A2}$$

where UT is the universal time (hours), E_o is the time of ephemeris transit (in hours, and available from the Almanac), ΔE_o (seconds) is the

difference of E_o for two successive days, the factor of 15 converts hours into degrees, and Long is the longitude (degrees) of the local receiving station. D_o is the solar declination in degrees, and ΔD_o is the difference (in seconds of arc) of D_o for two successive days.

The principal sources of error are the measurement of time and the measurement of ϕ. The errors in all other parameters are of negligible size and may legitimately be ignored.

The error in δ, $d\delta$, is given by:

$$d\delta = \pm (d\theta_S{}^2 + d\theta_N{}^2)^{\frac{1}{2}}$$

where $d\theta_S$ and $d\theta_N$ are the errors in θ_S and θ_N respectively. $d\theta_S$ results from errors in HA and D which come from the error in the time, UT. This error is estimated to be ± 1 sec. By differentiating A1 and A2 it is seen that

$$d(HA) = d(UT)$$

all other terms having negligible contribution, just as the value of dD. Since d(UT) is ± 1 sec., then d(HA) is ± 0.25 min arc.

From equation 2.2:

$$d\theta_S = \pm \frac{\cos(HA)\cos(D)}{\sin(\theta_S)} d(UT)$$

and is dependent on time. Consider an example from 09 May 1971:

UT = 15.00

D = 17.3°

HA = -35.5°

This gives $\theta_S = 123.6°$ which, in turn, gives $d\theta_S = \pm 0.23$ min. arc. From this discussion, a value of ± 0.25 min. arc is very reasonable to assume.

From equation 2.1:

$$d\theta_N = \pm \frac{\lambda}{d} \frac{d\phi}{\sin(\theta_N)}$$

The Gerber data reduction scaler gives digital readouts to the nearest 0.01 inch, and the chart paper size (for the solar records) in 4.5 inches. It was felt that the chart readings are reproducible to $\pm$ 0.02 inches. This gives $d\phi = 0.02/45 = 4.4 \times 10^{-3}$.

Using the data from the previous example, and an antenna separation of 49.4 wavelengths,

$$d\theta_N = \pm 0.4 \text{ min. arc.}$$

This gives

$$d\delta = \pm (0.25^2 + 0.4^2)^{\frac{1}{2}}$$

$$\simeq \pm 0.5 \text{ min arc}$$

This value is felt to be a reasonable estimate of the error involved in the 50 MHz interferometer readings. The records at 150 MHz have somewhat less error in $d\theta_N$ because of the increased value of d/λ, and so the error $d\delta_{(150\ \text{MHz})} \simeq 0.3$ min. arc.

This gives $\theta_S = 123.6°$ which, in turn, gives $d\theta_S = \pm 0.23$ min. arc. From this discussion, a value of ± 0.25 min. arc is very reasonable to assume.

From equation 2.1:

$$d\theta_N = \pm \frac{\lambda}{d} \frac{d\phi}{\sin(\theta_N)}$$

The Gerber data reduction scaler gives digital readouts to the nearest 0.01 inch, and the chart paper size (for the solar records) in 4.5 inches. It was felt that the chart readings are reproducible to $\pm$ 0.02 inches. This gives $d\phi = 0.02/45 = 4.4 \times 10^{-3}$.

Using the data from the previous example, and an antenna separation of 49.4 wavelengths,

$$d\theta_N = \pm 0.4 \text{ min. arc.}$$

This gives

$$d\delta = \pm (0.25^2 + 0.4^2)^{\frac{1}{2}}$$

$$\simeq \pm 0.5 \text{ min arc}$$

This value is felt to be a reasonable estimate of the error involved in the 50 MHz interferometer readings. The records at 150 MHz have somewhat less error in $d\theta_N$ because of the increased value of d/λ, and so the error $d\delta_{(150\ MHz)} \simeq 0.3$ min. arc.

REFERENCES

Beer, T., (1972), Atmospheric waves and the ionosphere, Contemp. Phys., 13, 247-271.

Beynon, W.J.G., (1948), Evidence of horizontal motion in region F_2 ionization, Nature, 162, 887.

Bowman, G.G., (1968), Movements of ionospheric irregularities and gravity waves, J. Atmos. Terr. Phys., 30, 721-734.

Bramley, E.N., (1953), Direction finding studies of large-scale ionospheric irregularities, Proc. Roy. Soc. London, A, 220, 39-61.

Bramley, E.N. and W. Ross, (1951), Measurements of the direction of arrival of short radio waves reflected at the ionosphere, Proc. Roy. Soc. London, A, 207, 251-267.

Chan, K.L., and O.G. Villard, Jr., (1962), Observation of large-scale travelling ionospheric disturbances by spaced-path high-frequency instantaneous-frequency measurements, J. Geophys. Res., 67, 973-988.

Cooley, J.W., and J.W. Tukey, (1965), An algorithm for the machine calculation of complex Fourier series, Math. of Computation, 19, 297-301.

Curry, M.J., (1973), Internal gravity waves of tropospheric origin, Ph.D. Thesis, University of Western Ontario, London, Canada.

Davies, K., (1965), Ionospheric radio propagation, National Bureau of Standards Monograph 80.

Davies, K., and D.M. Baker, (1966), On frequency variations of ionospherically propagated H.F. radio signals, Radio Sci., 1, 545-556.

Davies, K., and J.E. Jones, (1971), Ionospheric disturbances in the F2 region associated with severe thunderstorms, J. Atmos. Sci., 28, 254-262.

Davies, M.J., and A.V. DaRosa, (1969), Travelling ionospheric disturbances originating in the auroral oval during polar substorms, J. Geophys. Res., 74, 5721-5735.

Dixon, A.F., and C.E. Livingstone, (1969), RF phase comparator for angle of arrival and Faraday rotation measurements, Centre for Radio Science, University of Western Ontario, London, Canada, Report HA-13.

Forman, M., (1966), Fast Fourier transform technique and its application to Fourier spectroscopy, J. Opt. Soc. Am., 56, 978-979.

Francis, S. H., (1973), Acoustic-gravity modes and large-scale travelling ionospheric disturbances of a realistic, dissipative atmosphere, J. Geophys. Res., 78, 2278-2301.

Geisler, J. E., (1966), Atmospheric winds in the middle latitude F-region, J. Atmos. Terr. Phys., 28, 703-720.

Geisler, J. E.,(1967), A numberical study of the wind system in the middle thermosphere, J. Atmos. Terr. Phys., 29, 1469-1482.

Gentlemen, W. M., and G. Sande, (1966), Fast Fourier transforms - for fun and profit, Proc. Fall Joint Computer Conference, 563-578.

Georges, T. M., (1967), Ionospheric effects of atmospheric waves, E.S.S.A. Tech. Rept. IER 57-ITSA 54.

Georges, T. M., (1968), HF Doppler studies of travelling ionospheric disturbances, J. Atmos. Terr. Phys., 30, 735-746.

Hartz, T. R., and R. L. Hutchison, (1961), On the measurement of the angle of arrival of solar radiations at meter wavelengths, 1. A method for locating apparent radiation sources in the solar corona, D.R.T.E. Report No. 1057-1.

Heisler, L. H., (1958), Anomalies in ionosonde records due to travelling ionospheric disturbances, Aust. J. Phys., 11, 79-90.

Heisler, L. H., (1962), Observation of movement of perturbations in the F-region, J. Atmos. Terr. Phys., 25, 71-96.

Herron, T. J., (1973), Phase velocity disperson of F-region waves, J. Atmos. Terr. Phys., 35, 101-124.

Hewish, A., (1952), The diffraction of galactic radio waves as a method of investigating the irregular structure of the ionosphere, Proc. Roy. Soc. London, A, 214, 494-514.

Hines, C. O., (1960), Internal atmospheric gravity waves at ionospheric heights, Can. J. Phys., 38, 1441-1481.

Hines, C. O., and R. R. Rao, (1968), Validity of three-station methods of determining ionospheric motions, J. Atmos. Terr. Phys., 30, 979-993.

Jones, J., and G. F. Lyon, (1974), The focussing of radio waves by large scale ionospheric irregularities, J. Atmos Terr. Phys. 36, 461-473.

Kundu, M. R., (1965), Solar Radio Astronomy, Interscience (a division of John Wiley and Sons), New York, 1965.

Lawrence, R. S., and J. L. Jespersen, (1961), Refraction effects of large-scale ionospheric irregularities observed at Boulder, Colorado, Space Research II, Proc. 2ND Int. Sp. Sci. Symp., 277-284.

Little, A. G., and R. Payne-Scott, (1951), The position and movement on the solar disk of sources of radiation at a frequency of 97 Mc/s. I. Equipment, Aust. J. Sci. Res. A4, 489-507.

Litva, J., (1972), Observations of travelling ionospheric disturbances at London, Canada, NATO Advisory Group for Aerospace Research and Development, Conference on Effects of Atmospheric Acoustic Gravity Waves on Electromagnetic Waves Propogation.

Lyon, G. F., and J. A. D. Holbrook, (1972), The focussing effect on satellite radio observations due to travelling ionospheric disturbances, Space Research XII, 1143-1147.

MacDougall, J., (1972), F-region travelling disturbances over Jamaica, Space Res. XII, 1133-1142.

Midgley, J. E., and H. B. Liemohn, (1966), Gravity waves in a realistic atmosphere, J. Geophys. Res., 71, 3729-3748.

Munro, G. H., (1959), Travelling disturbances in the ionosphere, Proc. Roy. Soc. London, A, 202, 208-223.

Munro, G. H., (1953), Reflections from irregularities in the ionosphere, Proc. Roy. Soc., London, A, 219, 447-463.

Munro, G. H., (1958), Travelling ionospheric disturbances in the F-region, Aust. J. Phys., 11, 91-112.

Munro, G. H., and L. H. Heisler, (1956), Divergence of radio rays in the ionosphere, Aust. J. Phys., 9, 359-372.

2 2

OF/DE

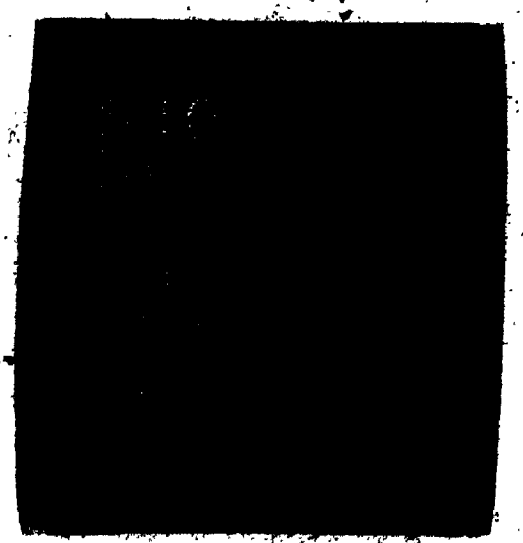

Pierce, J. A., and H. R. Mimno, (1940), The reception of radio echoes from distant ionospheric irregularities, Phys. Rev., 57, 95-105.

Pitteway, M. L. V., and C. O. Hines, (1963), The viscous damping of atmospheric gravity waves, Can. J. Phys., 41, 1935-1948.

Price, R. E., (1954), Travelling disturbances in the ionosphere, in Rept. Phys. Soc. Conf. on Phys. of the Ionosphere, London, 1954, pp. 181-190.

Rao, N. N. and K. C. Yeh, (1968), Large-scale ionospheric irregularities deduced from Faraday rotation observations at three stations, Space Res. VIII, 413-419.

Rao, N. N.,G. F. Lyon, and J. A. Klobuchar, (1969), Acoustic waves in the ionosphere, J. Atmos. Terr. Phys., 31, 539-454.

Reddi, C. R., and B. R. Rao, (1971), Characteristics of travelling ionospheric perturbations over Waltair using phase path technique, J. Atmos. Terr. Phys., 33, 251-266.

Thome, G. D., (1964), Incoherent scatter observations of travelling ionospheric disturbances, J. Geophys. Res., 60, 4047-4049.

Thome, G., (1968), Long-period waves generated in the polar ionosphere during the onset of magnetic storms, J. Geophys. Res., 73, 6319-6336.

Titheridge, J. E., (1963), Large-scale irregularities in the ionosphere, J. Geophys. Res., 68, 3399-

Titheridge, J. E., (1968), Periodic disturbances in the ionosphere, J. Geophys. Res., 73, 243-252.

Toman, K., (1955), Movement of the F-region, J. Geophys. Res., 60, 57-70.

Turnbull, R. M., and P. A. Forsyth, (1965), Satellite studies of isolated ionospheric irregularities, Can. J. Phys., 43, 800-817.

Tveten, L. H., (1961), Ionospheric motions observed with high frequency backscatter sounders, J. Res. NBS, 65D, 115-127.

Vasseur, G., C. A. Reddy, and J. Testud, (1972), Observations of waves and travelling disturbances, Space Res. XII, 1109-1131.

Vasseur, G., and P. Waldteufel, (1969), Thomson scatter observations of a gravity wave in the ionospheric F-region, J. Atmos. Terr. Phys., 31, 885-888.

Villasenor, A. J., (1968), Digital spectral analysis, NASA Tech. Note D4510.

Warwick, J. W., (1968), A model for Type IV emission in the solar burst of June 9, 1959 at decametric wavelengths, Solar Phys., 5, 111-117.

Webster, A. R., (1972), Power spectrum analysis of ionospheric data, Centre for Radio Science, University of Western Ontario, London, Canada, Report HA-21.

Wickersham, A. F., Jr., (1965), A ducted gravity wave interpretation of travelling ionospheric disturbances detected by a narrow beam, slewable backscattering radar, J. Geophys. Res., 70, 1729-1735.

Wild, J. P., K. V. Sheridan, and A. A. Neylan, (1959), An investigation of the speed of the solar disturbances responsible for type III radio bursts, Aust. J. Phys., 12, 369-398.

Winacott, E. L., (1961), On the measurement of the angle of survival of solar radiations at meter wavelengths 2. A high-resolution direction finding interferometer, D.R.T.E. Report No. 1057-2.

Winacott, E. L., (1963), On the measurement of the angle of arrival of solar radiations at meter wavelengths (U). An improved high-resolution direction - finding solar interferometer system, D.R.T.E. Report No. 1057-3.